Cretaceous Research 103 (2019) 104167

Contents lists available at ScienceDirect

Cretaceous Research

journal homepage: www.elsevier.com/locate/CretRes

Possible Late Cretaceous dromaeosaurid eggshells from South Korea: A new insight into dromaeosaurid oology

Seung Choi, Yuong-Nam Lee*

School of Earth and Environmental of Sciences, Seoul National University, Seoul, 08826, South Korea

ARTICLE INFO

Article history:
Received 24 January 2019
Received in revised form
17 May 2019
Accepted in revised form 21 June 2019
Available online 27 June 2019

Keywords:
Dinosaur egg
Dromaeosauridae
EBSD
Late Cretaceous
Eggshell phylogeny
Wido Volcanics

ABSTRACT

Among non-avian maniraptoran eggshells, oofamilies Prismatoolithidae and Elongatoolithidae are usually associated with troodontid and oviraptorosaur dinosaurs, respectively. However, dromaeosaurid eggshells are poorly known so far except for one possible *Deinonychus* egg associated with the gastralia of *Deinonychus*. Since then, some *Deinonychus* eggshell-like non-prismatoolithid and non-elongatoolithid maniraptoran eggshells have been reported including oogenera *Reticuloolithus* and *Montanoolithus*. Here we report a new ootaxon *Reticuloolithus acicularis* oosp. nov. from the Upper Cretaceous Wido Volcanics in South Korea. *R. acicularis* is characterized by reticulate ornamentation, an acicular mammillary layer, the continuous layer composed of two sublayers, and no external zone. EBSD analysis shows that *R. acicularis* has predominant low-angled grain boundaries, thereby its misorientation distribution is very similar to those of oviraptorosaurs and paleognaths. The comparisons to other maniraptoran ootaxa show that *R. acicularis* is morphologically very similar to *Deinonychus* eggshell, *Paraelongatoolithus*, and *Nipponoolithus*. The phylogenetic analysis based on a revised character matrix in this study shows that *R. acicularis*, *R. hirschi*, *Paraelongatoolithus*, and egg of *Deinonychus* make a polytomic relationship with the Elongatoolithidae. The new cladogram also raises some issues related to possible homology and homoplasy in the evolution of theropod eggshells. The possible dromaeosaurid affinity of *R. acicularis* is well matched with the body- and ichno-fossil record of the Cretaceous dromaeosaurids in East Asia. In addition, the low-angled misorientation of *R. acicularis* may imply the brooding behavior of the dromaeosaurids. Although dromaeosaurid eggshells have never been confirmed yet with embryos *in ovo*, the results of this study suggest that more possible dromaeosaurid eggshells can be clearly identified with EBSD analysis.

1. Introduction

The non-avian maniraptoran egg fossils have been intensively studied in non-avian dinosaurs (Varricchio and Jackson, 2016 and references therein). Among them, oofamilies Elongatoolithidae and Prismatoolithidae are widely reported in the world. The Elongatoolithidae is associated with oviraptorosaurs with strong evidence, specifically fossil embryos *in ovo* and frequent associations between adult body and egg fossils (Norell et al., 1995, 2001, 2018; Clark et al., 1999; Sato et al., 2005; Cheng et al., 2008; Weishampel et al., 2008; Fanti et al., 2012; Wang et al., 2016; Amiot et al., 2017; Pu et al., 2017). In the Prismatoolithidae, there are many oospecies whose egg-layers are unknown, but at least, *Prismatoolithus levis* is confirmed as an ootaxon of *Troodon formosus* based on an embryo *in ovo* and body-egg association (Jackson et al., 2010; Varricchio et al., 1997, 2002). Recently, van der Reest and Currie (2017) questioned the validity of taxon name *Troodon formosus*, but Varricchio et al. (2018) provided a reason to maintain its validity, which we followed in this study. Due to *Prismatoolithus levis*, almost all prismatoolithid eggs are usually interpreted as belonging to the derived non-oviraptorosaur maniraptorans closely related to troodontids (Tanaka et al., 2018).

On the other hand, the Dromaeosauridae is a sister group of the Troodontidae and they make a higher clade named Deinonychosauria together (Turner et al., 2012). The Deinonychosauria is most closely related to the Aves, which both comprise the Paraves (Sereno, 1997; Turner et al., 2012). Recently, the monophyly of the Deinonychosauria was challenged and suggested to be paraphyletic (Godefroit et al., 2013) or the Dromaeosauridae and Troodontidae make polytomic relationships with *Anchiornis, Archaeopteryx*,

* Corresponding author.
E-mail addresses: seung0521@snu.ac.kr (S. Choi), ynlee@snu.ac.kr (Y.-N. Lee).

https://doi.org/10.1016/j.cretres.2019.06.013
0195-6671/

Wellnhoferia, and *Xiaotingia* (Xu et al., 2017) (see also Brusatte et al., 2015). Nevertheless, it is still evident that the Dromaeosauridae and Troodontidae are most closely related to the Aves in the lineage of non-avian Maniraptora. Hence, dromaeosaurid eggs are very important to understand the eggshell evolution in derived non-avian Maniraptora.

Contrary to troodontid and oviraptorosaur eggshells, however, there are only a few studies on possible dromaeosaurid eggshells. Grellet-Tinner and Makovicky (2006) reported a partial egg and eggshells closely associated with gastralia of *Deinonychus* with a notion that they are the only egg material that can be associated with a dromaeosaurid with high probability. Since then, several *Deinonychus* eggshell-like non-prismatoolithid and non-elongatoolithid maniraptoran ootaxa have been reported (Table 1). Because they were morphologically different from the Prismatoolithidae and Elongatoolithidae but similar to *Deinonychus* eggshells, their potential egg-layers were inferred to be dromaeosaurids (Tanaka et al., 2016; Vila et al., 2017; Voris et al., 2018; Zelenitsky and Sloboda, 2005; Zelenitsky and Therrien, 2008a; Zelenitsky et al., 2017a, 2017b).

In South Korea, dinosaur body fossils are somewhat rare (Lee et al., 2001; Choi and Lee, 2017), but twelve dinosaur egg localities were found in several Cretaceous basins (Huh et al., 2006, 2014; Kim et al., 2011; Lee, 2003, 2017; Lee et al., 2007; Lee, 2008; Paik et al., 2004, 2012). A total of 577 dinosaur eggs with 90 clutches represents five different oofamilies (Lee, 2017). They are spheroolithid, faveoloolithid, dendroolithid, elongatoolithid, and ovaloolithid eggs (Huh et al., 2006; Paik et al., 2012) but many of them have not been studied yet in detail. The eggshells described in this study were found in the Wi Island, Buan County, one of the unstudied localities in South Korea. The material of this study shows strong morphological similarity with the Early Cretaceous *Deinonychus* eggshells and Late Cretaceous *Reticuloolithus hirschi*. Furthermore, it represents the second type of theropod eggs after the elongatoolithid eggs from South Korea (Kim et al., 2011; Huh et al., 2014). Therefore, this study aims to compare this new type of eggshells with possible dromaeosaurid eggshells in the world and, more importantly, to understand their phylogenetic relationships based on a newly revised character matrix. Furthermore, EBSD analysis was applied for revealing crystallographic features of the eggshells that may have a reproductive implication.

2. Geological setting

Cretaceous volcanic-influenced sedimentary basins are widely distributed in South Korea (Choi and Lee, 2017, fig. 1; Chough, 2013; Chough et al., 2000). The biggest basin is the Gyeongsang Basin in the southeastern part of the Korean Peninsula of which sediments were thought to be deposited since the Barremian, Early Cretaceous (Lee et al., 2018a, b). The deposition of the Cretaceous basins in Korean Peninsula was caused by oblique subduction direction of the Izanagi plate (Chough et al., 2000; but see also Kim et al., 2016 and Ryu and Lee, 2017 for alternative tectonic model). In the southwestern part of the Korean Peninsula, Cretaceous basins are aligned in NE-SW directions (e.g. the Eumsung, Jinan, Haenam, and Kyokpo basins) (Chough, 2013; Kwon et al., 2017 and references therein). The Wi Island is part of these volcanic-influenced sedimentary successions and situated in the Yellow Sea, 15 km west from the Kyokpo Basin (Fig. 1A).

The island is composed of the Wido Volcanics, which comprises four conformable subunits: the Daeri Andesite, Mangryeongbong Tuff, Beolgeumri Formation, and Ttandallae Tuff in ascending order (Fig. 1B; Ko et al., 2017; Koh et al., 2013). The Daeri Andesite is located at the southern coast of the island and mainly composed of andesite interbedded with sedimentary rocks. The Daeri Andesite can be subdivided into two subunits (Ko et al., 2017). The lower Daeri Andesite is mainly composed of siliciclastic sedimentary rocks which were interpreted to be deposited in a semi-arid floodplain environment, whereas the upper Daeri Andesite consists of aphyric to porphyritic andesite (Gihm et al., 2017). The egg fossils were found in the lower Daeri Andesite. The Mangryeongbong Tuff occupies the majority of the island and yielded a radiometric age of 86.63 ± 0.83 Ma (Coniacian–Santonian) (Ko et al., 2017). This delimitates the youngest age of the egg fossils in the Wido Volcanics. The Beolgeumri Formation comprises tuffaceous conglomerate, sandstone, mudstone, and black shale which were deposited by the pyroclastic density currents in the lacustrine environment (Gihm and Hwang, 2014, 2016). The Ttandalle Tuff is the uppermost subunit of the Wido Volcanics and is composed of breccias and lapilli tuff deposited by pyroclastic density currents (Ko et al., 2017).

The fossil eggs of the lower Daeri Andesite occur in sub-vertical (upper part of the section) and sub-horizontal outcrops (lower part of the section) in the eastern coastal area of Wi Island (Fig. 2A). Homogeneous reddish siltstone with intercalated calcrete nodules is the most dominant lithofacies at the fossil site. The grain size of the siltstone ranges from 23 to 70 μm with an average of 48 μm. Grains are moderate to well sorted. The white to ivory calcite-filled joints and small-scale syndepositional normal faults are commonly observed at the fossil locality (Gihm et al., 2017).

3. Material and methods

Two types of dinosaur eggs and an enigmatic archosaur egg were discovered at the site. The two kinds of dinosaur eggs are easily distinguished from each other in the field by eggshell thickness. The thicker eggshells (1.65 mm in thickness) named *Propagoolithus widoensis* are widely distributed in both sub-horizontal and sub-vertical outcrops of the sedimentary section of the site (Kim et al., 2019). The thinner eggshells of this study occur mainly in the sub-horizontal outcrop as fragmentary pieces, which do not exceed 1 mm in thickness (Fig. 2B). Occasionally, both eggshells are found at the same spot and horizon, implying that both eggs coexisted spatiotemporally unless the time-averaging effect was severe in this locality (Behrensmeyer et al., 2000; Botfalvai et al., 2017). At least twelve eggshell fragments were found in the sub-horizontal outcrop (Fig. 2C). Although they are small pieces (less than 1 cm in length) and coated by calcite at both surfaces, some of them were well preserved enough to see the mammillary layer in the field.

Ten eggshell fragments were collected from a boulder at the site and an eggshell fragment was excavated from the sub-horizontal outcrop. The stereomicroscope and SEM observation confirmed that all eggshells are of the same type. The surface ornamentation was examined by using a stereomicroscope (Leica M165C). Eight thin sections were prepared following the procedure of Quinn (1994). The thin sections were examined with Nikon Eclipse LV100N POL and Nikon Optiphot-2 POL polarized light microscopes. Three fresh radial sections and the surface of two eggshells were coated with carbon and their images were captured with SEM (JEOL JSM-7100F) at 15.0 kV. Additionally, the electron backscatter diffraction (EBSD; an auxiliary device of SEM) analysis was applied to the samples following the methods of Moreno-Azanza et al. (2013) and Choi et al. (2019). The inverse pole figure (IPF) map, grain boundary map, misorientation histogram, and the ruggedness of the squamatic ultrastructure are presented following Choi et al. (2019). The CL (cathodoluminescence) images were taken by CL mode of FE-EPMA (JEOL JXA-8530F) using the same specimen made for EBSD analysis. FE-SEM and FE-EPMA are housed in the

Table 1
Possible dromaeosaurid eggshells in the literature. Abbreviations: ML, Mammillary layer; CL, Continuous layer.

Taxon/Ootaxon	Locality	Age/Formation	Egg size (mm)	Eggshell thickness (mm)	Ornamentation	ML morphology	ML/CL boundary	ML:CL	Pore type	Reference
Deinonychus antirrhopus	Cashen Pocket, Montana, USA	Aptian–Albian/Cloverly	? × (65–70)	0.44 (average–) 0.60	Anastomosing bumps and ridges	Acicular	Abrupt	1:2.35–2.94	?[a]	Grellet-Tinner and Makovicky (2006)
Nipponoolithus ramosus	Kamitaki, Hyogo, Japan	Albian/'Lower Formation' of the Sasayama Group	?	0.37–0.53; 0.44 (average)	Branching ridges	Acicular or wedges	Abrupt	1:2–1:4	?	Tanaka et al. (2016)
Paraelongatoolithus reticulatus	Tiantai, Zhejiang, China	Cenomanian –Turonian/ Chichengshan	170 × 72	0.50–0.60; 0.70 –0.85 (with ornamentation)	Reticulate	Acicular or wedges	Abrupt	1:2	angusticanaliculate	Wang et al. (2010)
Reticuloolithus acicularis	Wi Island, North Jeolla Province, Korea	Coniacian–Santonian/ Wido	?	0.530–0.776; 0.649 (average)	Reticulate	Acicular	Abrupt	1:2.2–1:2.6	angusticanaliculate	**This study**
Reticuloolithus hirschi	Dinosaur Provincial Park, Canada	Campanian/Dinosaur Park	?	0.35–0.50[b]	Reticulate	Acicular	Abrupt	1:2–1:3	?	Zelenitsky and Sloboda (2005); Zelenitsky and Therrien, (2008a)
Montanoolithus strongorum	Blackfeet Reservation, Montana, USA	Campanian/Two Medicine	125 × 60	0.7–0.85	Anastomosing	Wedges	Gradational	1:2	?	Voris et al. (2018); Zelenitsky and Therrien, (2008a)
Montanoolithus labadousensis	Les Labadous, Occitanie, France	Maastrichtian/Marnes rouges de la Maurine	?	0.6–0.7; 0.8 –0.95 (with ornamentation)	Anastomosing	Wedges	Gradational	1:3	angusticanaliculate	Vila et al. (2017)

[a] In original paper, the shape of 'pore canal' is described as "straight with an elbow close to the surface". However, the 'pore canal' size (15 μm) is inconsistent with pore aperture size (130 μm × 60 μm) and the opening shape of putative 'pore canal' in radial view is not funnel-shaped. Thus, we think that the putative 'pore canal' in radial view in this paper would be a simple crack (Choi et al., 2019).
[b] The thickness (0.76 mm) presented in Zelenitsky & Sloboda (2005) is a mistake because the thickness of the eggshell in Zelenitsky & Sloboda (2005, fig. 20.1A) is around 0.3 mm. Thus, we followed Zelenitsky & Therrien (2008a) for measurements.

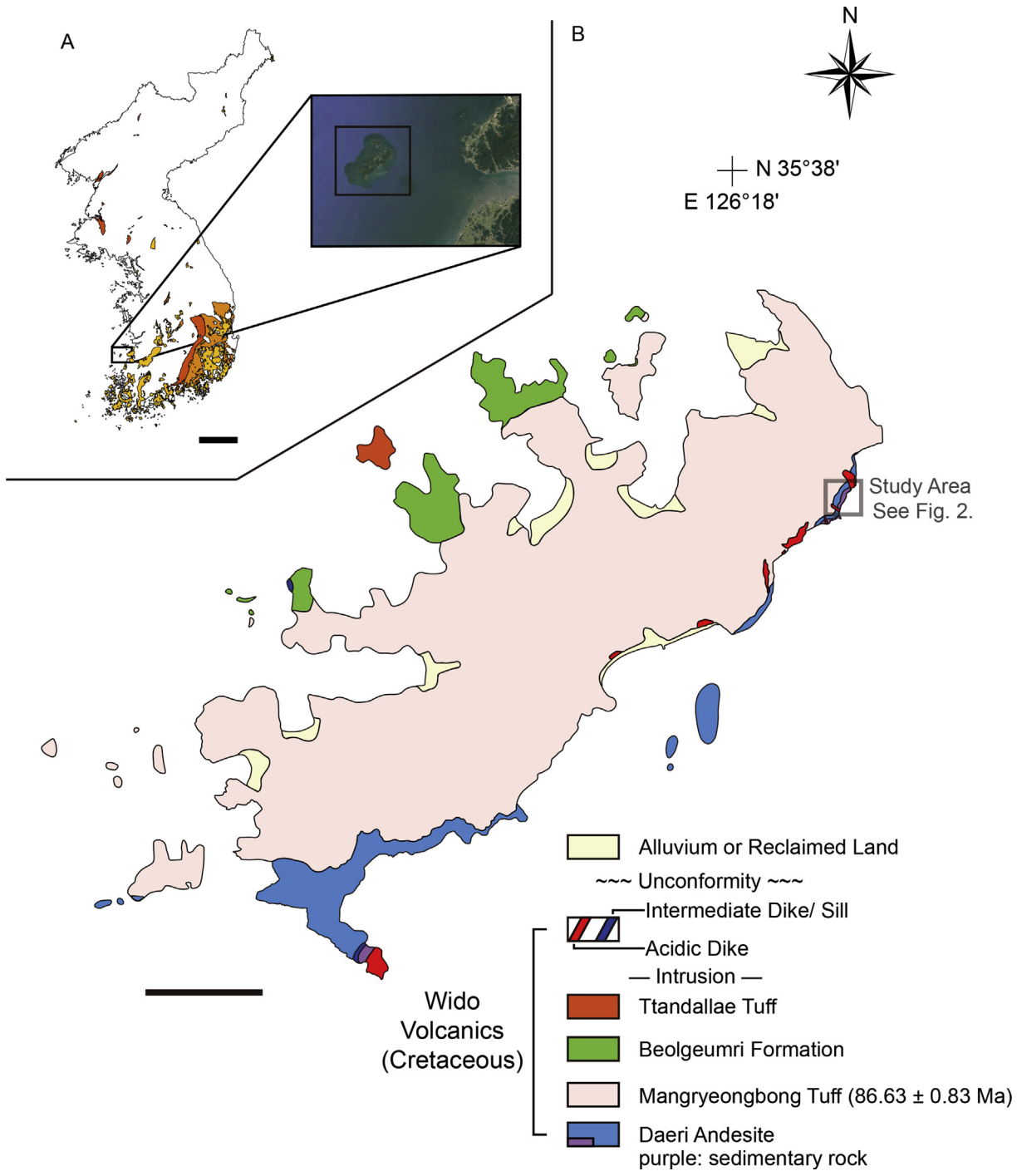

Fig. 1. Location and geological map of the Wi Island. (A) A map of the Korean Peninsula showing the location of the Wi Island (modified from Choi and Lee, 2017) with Cretaceous basins (colored). (B) An enlarged geological map of the Wi Island modified from Ko et al. (2017); Koh et al. (2013). The Wido Volcanics is subdivided into four conformable members and two kinds of dinosaur egg fossils and one archosaur egg fossil were discovered in the lower Daeri Andesite. More detailed fossil locality information is provided in Fig. 2. Scale bars equal 100 km (A) and 1 km (B).

School of Earth and Environmental Sciences and National Center for Inter-University Research Facilities, Seoul National University, respectively. The microscopic measurements were made using ImageJ from the PLM, SEM, CL, and EBSD images 30 times and the average was presented. The egg dimension was estimated by using the method of Ribeiro et al. (2014). Descriptive terminology followed Mikhailov (1997a).

We used the data matrix of Fernández and Salgado (2018), which is an extended version of Zelenitsky (2004), Tanaka et al. (2011), and Vila et al. (2017). We found miscoded character states from the original matrices, thus some modifications were applied to the most recently published matrix of Fernández and Salgado (2018) for our new phylogenetic analysis. The cladistic analysis of ootaxa was carried out with TNT v.1.5 (Goloboff and Catalano,

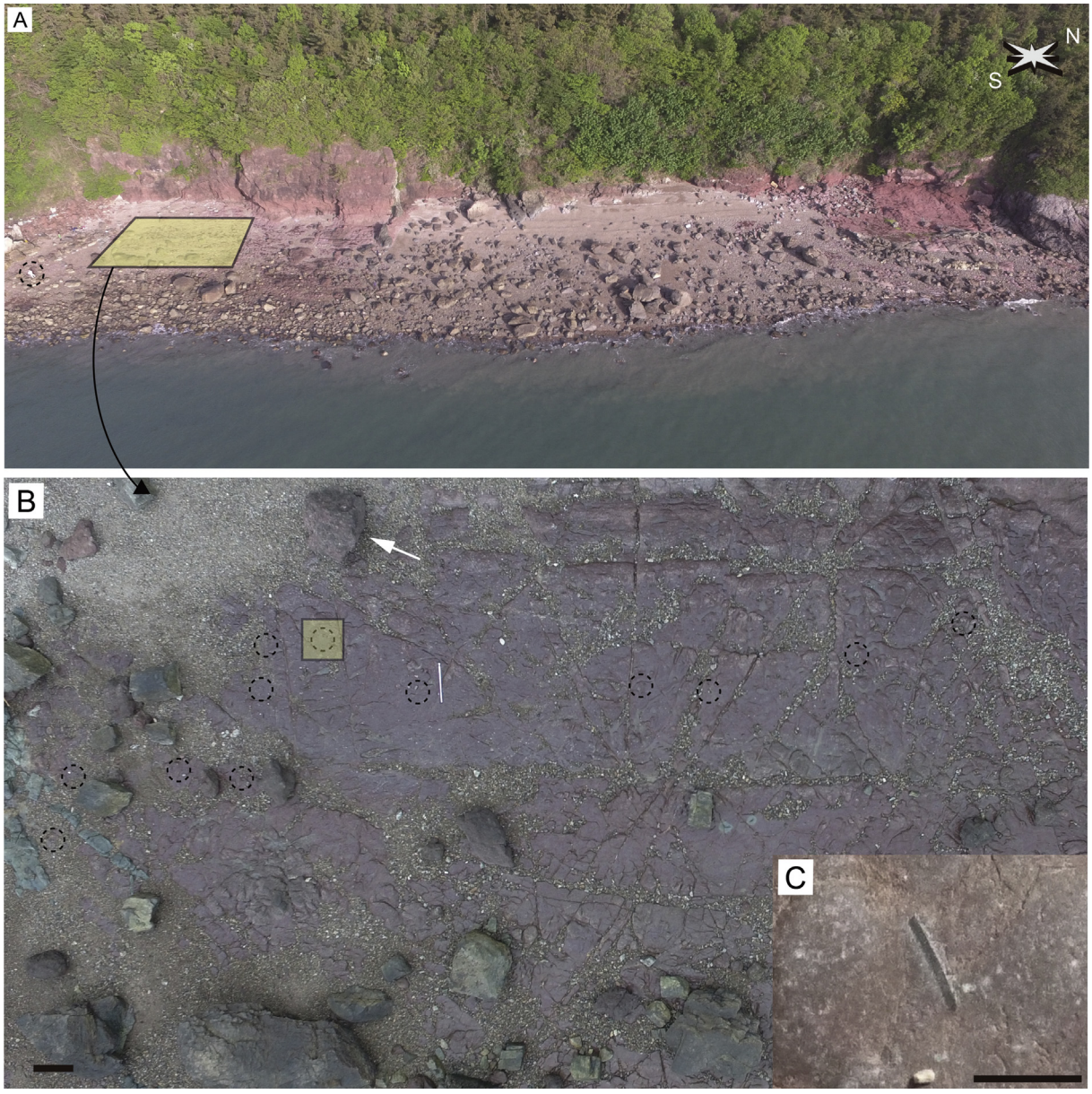

Fig. 2. Egg site. (A) Aerial view of the study area. Sub-vertical and sub-horizontal outcrops are well developed along the coastal area. (B) Locations of the *Reticuloolithus acicularis* oosp. nov. in a shaded area of (A). All of *R. acicularis* eggshells were found on the surface of the sub-horizontal outcrop and a boulder (a white arrow). The specimens from the isolated boulder were used for this study. Many fragments of *R. acicularis* are associated with another type of eggshells (Kim et al., 2019). (C) *R. acicularis* in a square of (B). A man in a dotted circle for scale (A); Scale bars equal 1m (B) and 1 cm (C).

2016). The setting of the TNT when we constructed the cladogram are as follows: a traditional heuristic tree search; 10 replicates of Wagner trees; saving 10 trees per replication for tree bisection reconnection (TBR) branch swapping (i.e. default setting of 'traditional' search).

Institutional abbreviations. IGM, Mongolian Institute for Geology, Ulaanbaatar, Mongolia; MOR, Museum of the Rockies, Bozeman, Montana, USA; SNUVP, Paleontological Laboratory of Seoul National University, Seoul, South Korea.

Technical abbreviations. CL, cathodoluminescence; EBSD, electron backscatter diffraction; EI, elongation index; FE-EPMA, field emission electron probe microanalyzer; H, arc height; h, height; IPF, inverse pole figure; ML, mammillary layer; PLM, polarized light microscopy; SEM, scanning electron microscopy; t, eggshell thickness; W, width.

4. Systematic paleontology

Oofamily incertae sedis

Oogenus ***Reticuloolithus*** Zelenitsky and Sloboda, 2005.

Emended diagnosis. Eggshell with two layers; Eggshell thickness 0.35–0.78 mm; Ratio of the mammillary to continuous layers 1:2–1:3; Cryptoprismatic shell unit; Acicular mammillary layer; An abrupt and straight boundary between the mammillary and continuous layers; Linear (non-undulating) growth lines in the continuous layer; Ornamentation composed of reticular network of ridges.

Remarks. The eggshell thickness of *Reticuloolithus hirschi* is 0.35–0.50 mm (Zelenitsky and Therrien, 2008a), which was originally reported as 0.60–0.94 mm (Zelenitsky and Sloboda, 2005).

Oospecies. *Reticuloolithus acicularis* oosp. nov
Figs. 3–7

Etymology. The oospecific name "*acicularis*" refers to the acicular structure of the mammillary layer in Latin.
Holotype. SNUVP 201601, a thin section housed at the School of Earth and Environmental Science, Seoul National University.
Referred specimens. Macroscopic specimen (SUNVP 201608); Thin sections (SNUVP 201602 and 201603); Mounted specimens for SEM observation (SNUVP 201604, 201605, and 201606); Specimen for CL analysis (SNUVP 201607); Specimen for EBSD analysis (SNUVP 201607 and 201603).
Type locality and age. The holotype is from the lower Daeri Andesite of the Upper Cretaceous Wido Volcanics (Coniacian–Santonian), Wi Island, Buan County, North Jeolla Province, South Korea.

Diagnosis. An acicular mammillary layer confirmed by EBSD analysis (calcite radial ultrastructure with polygonal cross section); Eggshell thickness is 0.45–0.75 mm; Ratio of the mammillary to continuous layers is around 1:2.5; Type 1 misorientation distribution (*sensu* Choi et al., 2019).
Remarks. The EBSD analysis results are used for the oospecific diagnosis of *Reticuloolithus acicularis*. However, we anticipate that they could be used for the diagnosis of oogenus *Reticuloolithus* when the EBSD analysis is applied to and crystallographic data are drawn from *Reticuloolithus hirschi*.

Description
Taphonomic considerations. Taphonomic features were examined from the specimen in order not to misidentify the taphonomic imprints as biologically meaningful ones (Behrensmeyer et al.,

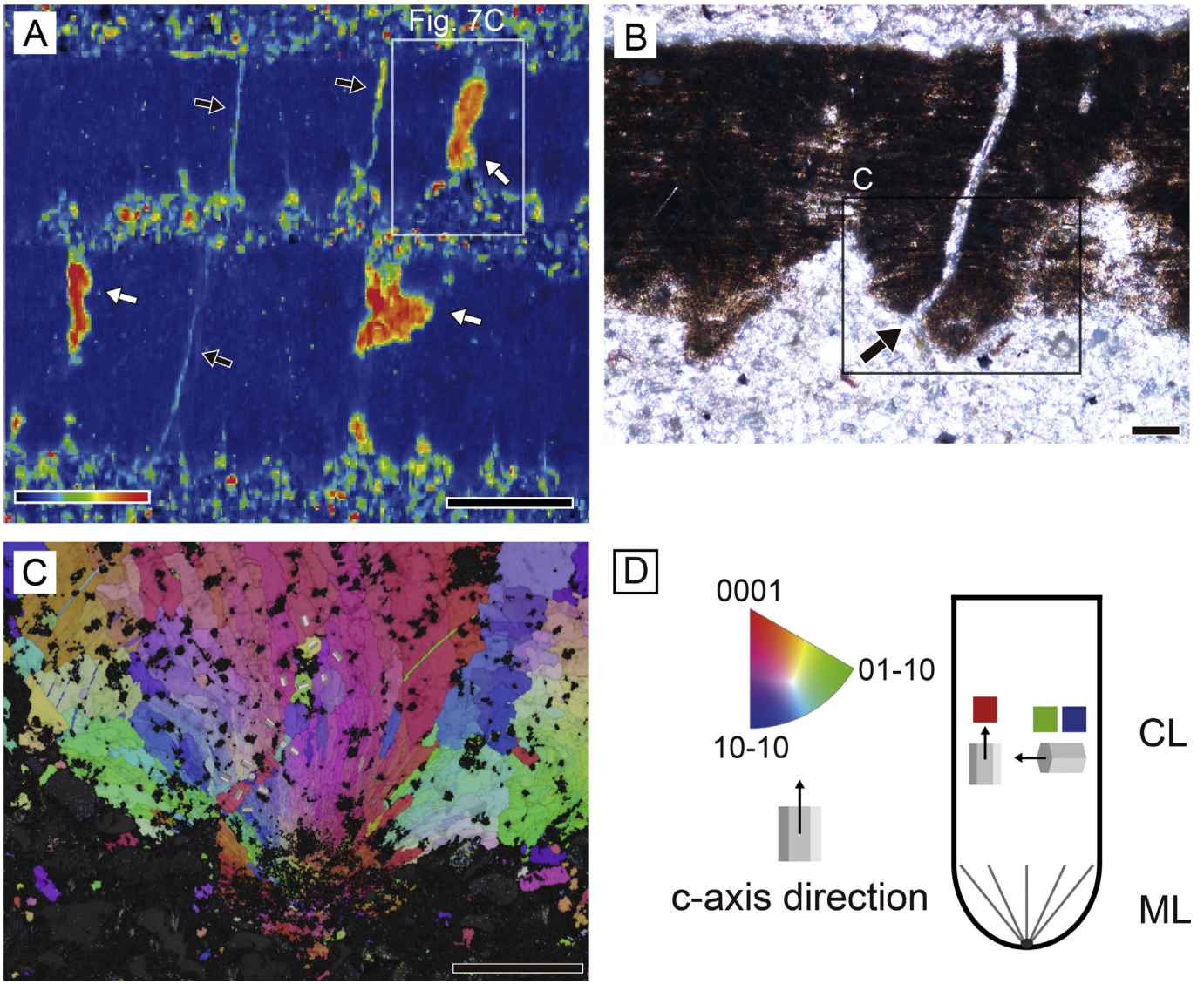

Fig. 3. Taphonomic consideration of *Reticuloolithus acicularis* oosp. nov. (A) CL micrograph showing the diagenetic effect caused by manganese ion (SNUVP 201607). White arrows mark potential pore canals, while black arrows point the cracks. Spectrum bar on the lower left corner shows CL intensity with reddish band stronger reactivity. (B) Thin section image of a crack (a black arrow) passing through a shell unit (SNUVP 201603). (C) EBSD image at the crack (SNUVP 201603). Note that calcite grains beside a crack maintain crystallographic continuity represented by hexagonal columns. (D) Inverse pole figure (IPF) map legend shows how to interpret EBSD IPF map. The calcite grains of which c-axis aligned perpendicular to the eggshell surface are colored red. In contrast, blue- and green-colored parts are equivalent to the calcite crystals that have horizontally aligned c-axis. ML and CL denotes mammillary layer and continuous layer, respectively. Scale bars (black ones) represent 500 μm (A) and 100 μm (B–C).

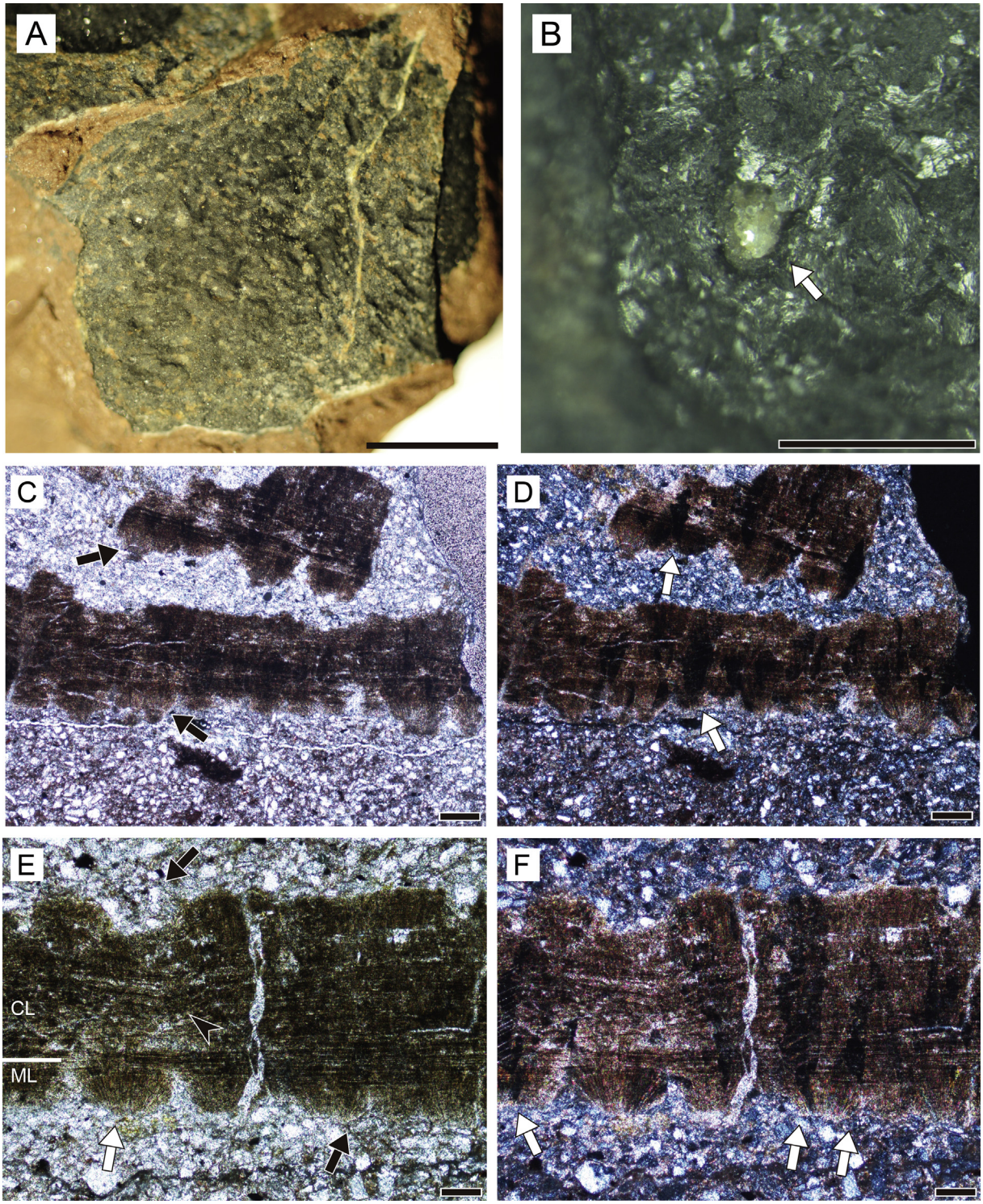

Fig. 4. Stereomicroscopic and PLM images of *Reticuloolithus acicularis* oosp. nov. (A) External surface shows net-like (*sensu* Zelenitsky, 2004) ornamentation (SNUVP 201608). (B) A pore canal (a white arrow) exposed in a weathered tangential section (SNUVP 201608). (C) Wide view of a radial thin section under normal light (SNUVP 201602). Note that not all mammillae are preserved. Black arrows point arc-shaped structure seen at the mammillary layer. (D) SNUVP 201602 under polarized light. Extinction patterns are fan- or column-shaped (white arrows). (E) Radial thin section under normal light (SNUVP, 201601, holotype). The boundary between the mammillary layer (ML) and continuous layer (CL) is abrupt (a white bar). Note acicular calcite radial structure (a white arrow). Indented pits and fused mammillae are irregularly distributed at the outer and inner surfaces, respectively (black arrows). Note slightly bended growth lines near the pit (a black arrowhead). (F) SNUVP 201601 under polarized light. Note the fan-like extinction pattern (white arrows). Scale bars represent 5 mm (A), 500 μm (B), 200 μm (C–D), and 100 μm (E–F).

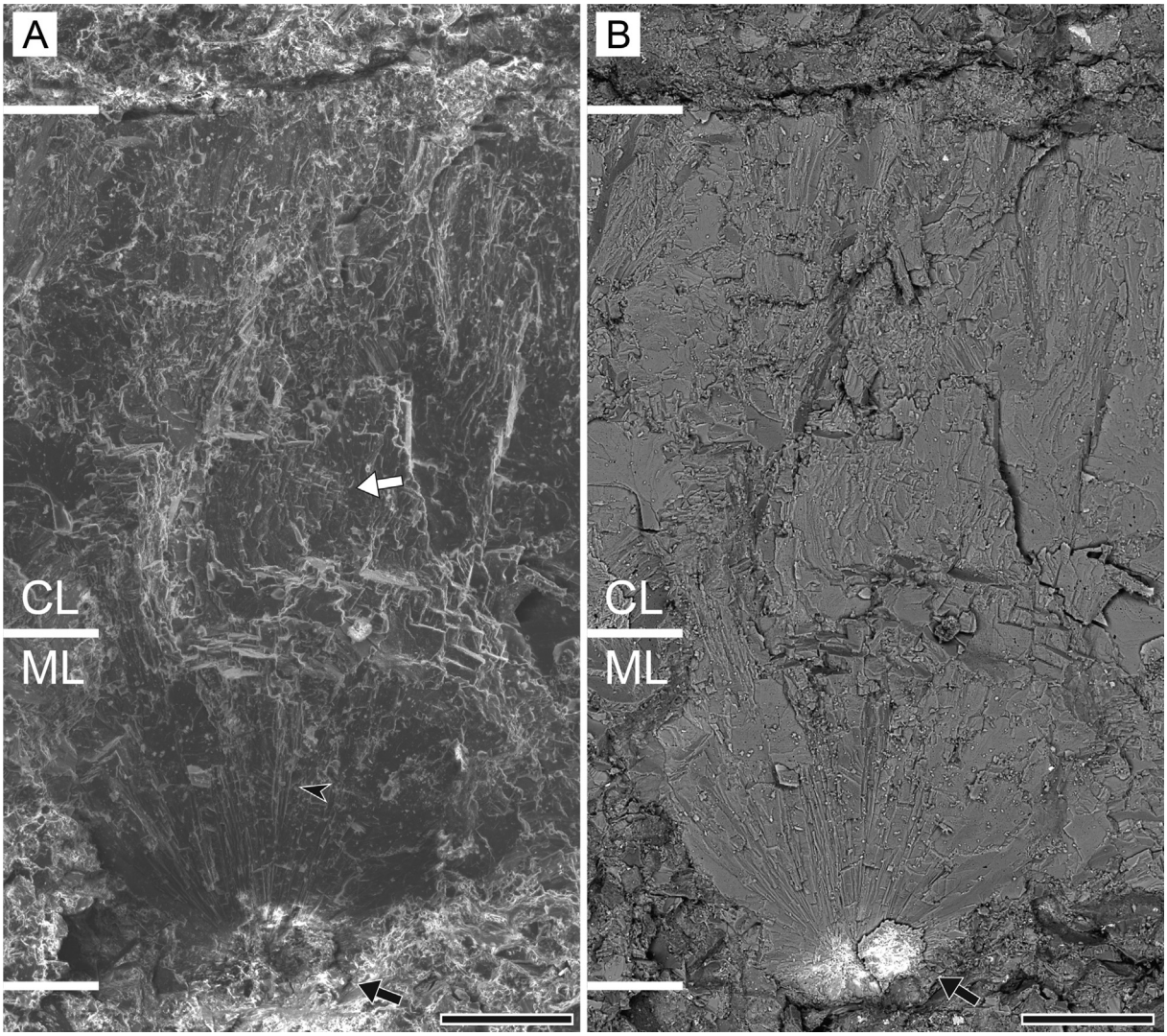

Fig. 5. SEM images of *Reticuloolithus acicularis* oosp. nov. in low magnification (SNUVP 201606). (A) Radial view in secondary electron mode. The eggshell is embedded in matrix and the boundary between the eggshell and matrix is marked by white bars. A white arrow points squamatic ultrastructure (see also Fig. 6F). A black arrow points eroded nucleation site, which is better preserved than others seen in thin sections. Note acicular calcite radial ultrastructure in a mammilla (a black arrowhead; Fig. 6E). (B) In backscattered electron mode. Note that bright signal marked by a black arrow was caused by the charging effect of the specimen, not by heavy minerals. Scale bars represent 100 μm (A–B).

2000; Choi et al., 2019; Grellet-Tinner et al., 2010; Moreno-Azanza et al., 2016). CL imaging can reveal the regions, which were affected by manganese ion, a typical substance associated with diagenesis (Machel, 1985; Grellet-Tinner et al., 2010; Kim et al., 2019). Thin oblique tubular and thick pore-like structures, affected by diagenesis, were observed with CL (Fig. 3A). Except for these, the eggshell did not show any significant diagenetic signal. An oblique tubular structure turned out to be cracks because there exists a crystallographic continuity besides the canal which is not observed in true pore canals of extant avian eggshells (Fig. 3B–C; Choi et al., 2019).

On the other hand, the external surface of the continuous layer is partially indented with irregular pits in some specimens (Fig. 4C–F). The similar structures were reported in weathered modern avian eggshells due to effects of pH, temperature (Clayburn et al., 2004), and/or microorganism (Smith and Hayward, 2010). Such pits may be an indirect evidence of subaerial exposure of the materials before burial. However, the bending of the growth lines is observable near the irregular pits in the outer part of eggshell like *Deinonychus* eggshell (Zelenitsky, 2004; pl. 6.14), *Continuoolithus canadensis* (Jackson et al., 2015, fig. 4B), and *Guegoolithus turolensis* (Spheroolithidae) from Spain (Moreno-Azanza et al., 2014a, fig. 2D). We interpret, thereby the irregular pits in radial view and the reticular outer surface of the specimen as the reflection of external ornamentation rather than a taphonomic trait.

Some eggshells are thinner without pits than others in radial view, implying that the outer part of eggshells may have been eroded (e.g. Varricchio et al., 2013) unless the difference corresponds to normal eggshell thickness variability across the egg (e.g. Funston and Currie, 2018, fig. 2; Jin et al., 2007, table 2). The inner part of the eggshell was less affected by diagenesis judging from the existence of well-preserved mammillary layer. It suggests that the inner part of eggshell was not heavily altered, but nevertheless, approximately two-thirds of the mammillae are partially worn or fused together which is reminiscent of weathered modern avian eggshells (Clayburn et al., 2004; Smith and Hayward, 2010) or the absorption of the mammillary layer during embryogenesis (Karlsson and Lilja, 2008).

Egg size estimation. Because only fragmentary eggshells are available, the egg size had to be estimated by using the curvature of eggshell fragments (Ribeiro et al., 2014). Because the

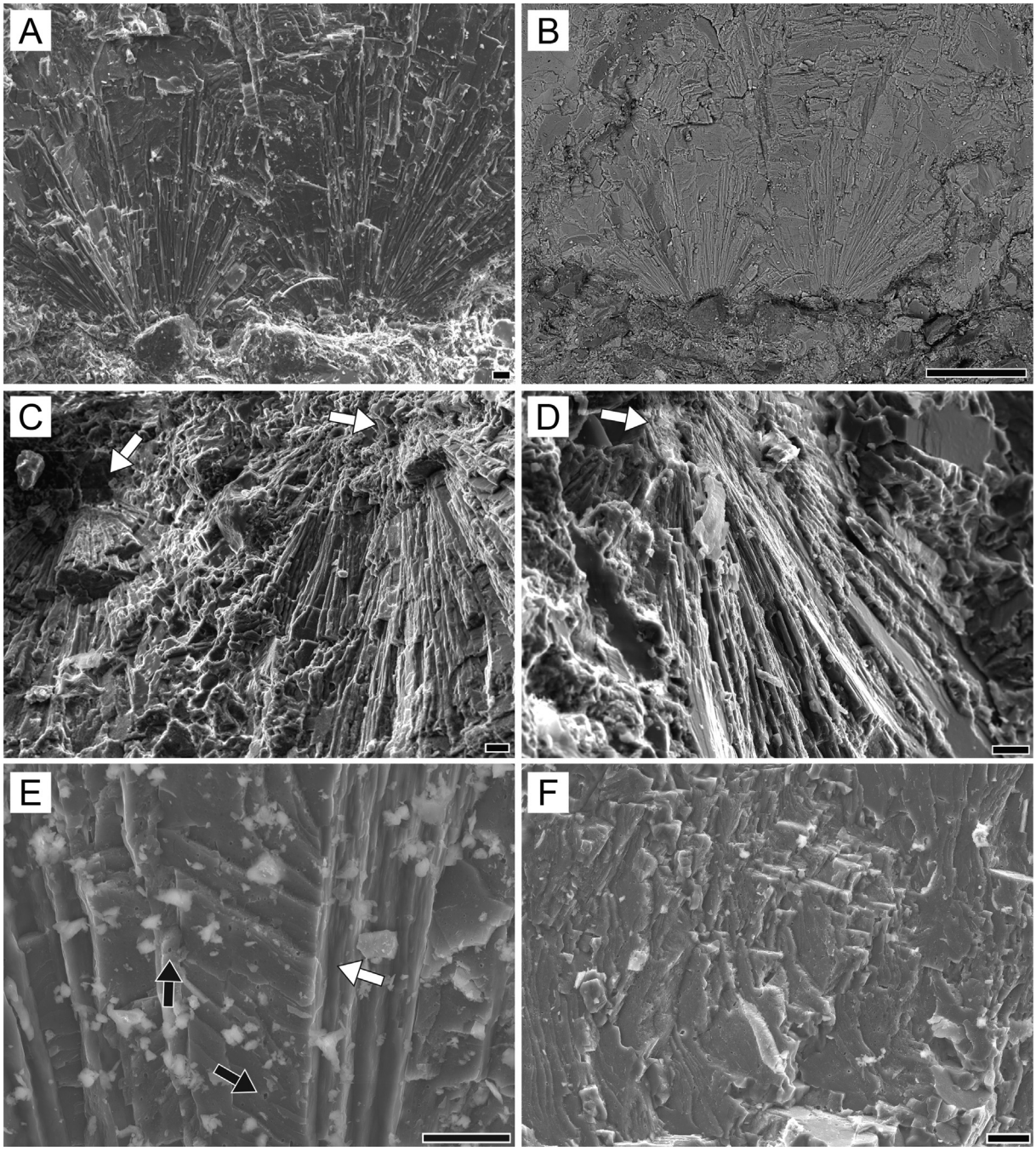

Fig. 6. SEM images of *Reticuloolithus acicularis* oosp. nov. in high magnification (A, B, E, and F, SNUVP 201606; C, 201605; D, 201604). (A) Radial view of acicular calcite radial ultrastructure that radiate from the nucleation center in the mammillary layer. (B) In backscattered electron mode. (C) Radial-tangential view of acicular calcite radial ultrastructure. Note the polygonal cross section of each calcite radial ultrastructure. White arrows point nucleation sites. (D) Lateral view of the mammillary layer. A nucleation site is marked by a white arrow. (E) Oblique tabular ultrastructure (a white arrow) is observed along with vesicles (black arrows) in calcite radial ultrastructure of the mammillary layer. (F) Squamatic ultrastructure just above the mammillary layer. Scale bars represent 100 μm (B) and 10 μm (A, C–F).

EI (elongation index) of *Reticuloolithus acicularis* is not known, we assumed a spherical shape because it is the simplest form that the size can be estimated. We measured three variables (W, h, and t) from each fragment (N = 19) and one variable (H, arc height) was calculated from other two variables (see Materials and methods of Ribeiro et al., 2014 for details). The result showed (Table S1) that if *R. acicularis* had a spherical shape, its radius would be around 23.3 mm (i.e. 46.6 mm in diameter). We further assumed that EI of *R. acicularis* was similar to that of *Paraelongatoolithus reticulatus* (EI = 170/72 = 2.36), which is another possible dromaeosaurid ootaxon (Table 1) whose egg dimensions are known. In this case, the estimated egg length and width are 75.7 mm and 32.1 mm, respectively (Ribeiro et al., 2014, eq. 4). The possible size of *R. acicularis* is much smaller than other maniraptoran eggshells and comparable to the smallest prismatoolithid *Prismatoolithus carboti* (70 mm × 30 mm; Garcia et al., 2000), *Triprismatoolithus stephensi* (family incertae sedis; 75 mm × 30 mm; Jackson and Varricchio, 2010), and belonoolithid *Belonoolithus garbani* (80 mm × 60 mm; Jackson and Varricchio, 2016).

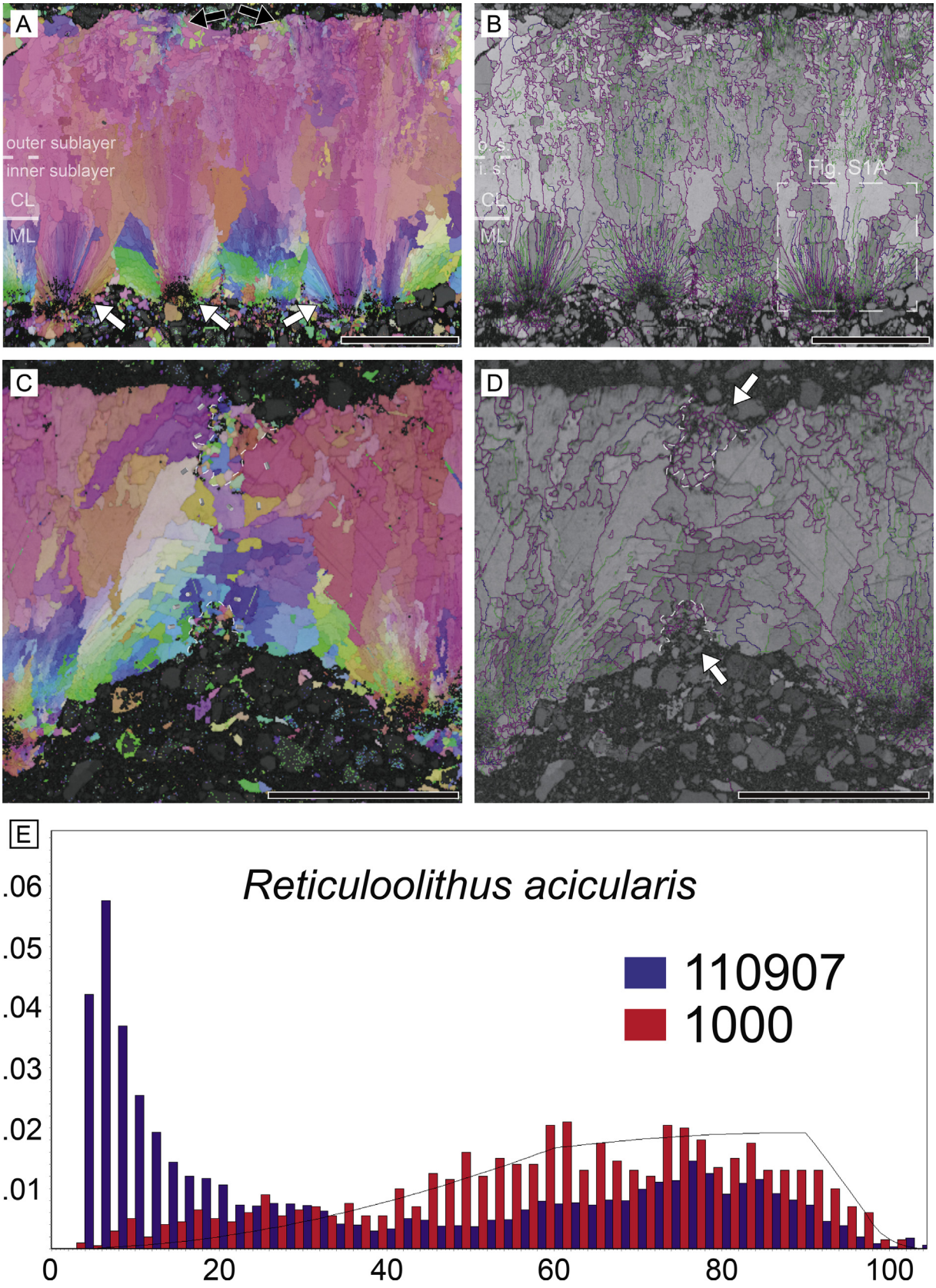

Fig. 7. IPF maps, grain boundary maps, and misorientation angle distribution of *Reticuloolithus acicularis* oosp. nov. (SNUVP 201607). See Fig. 3D for the meaning of grain colors in A and C. The green, blue, and purple lines in B and D mean the angles between the grains which are 5°–10°, 10°–20°, and >20°, respectively. (A) IPF map shows that the mammillary layer is usually fan-shaped. Calcite radial ultrastructure in the mammillary layer abruptly changes into blocky grains in the continuous layer. In the continuous layer, c-axis is aligned perpendicular to the eggshell surface but those of the mammillary layer are partly horizontally aligned (see green- and blue-colored grains). White arrows point arc-shaped structure which was not indexed in EBSD analysis (see also Fig. 3B; Fig. 4C). Black arrows mark possibly recrystallized regions. (B) Grain boundary map. Note abundant low-

Stereoscopic and PLM image. The outer surface of the eggshell is bumpy and weakly reticulated in the thickest piece (Fig. 4A). Only one pore canal can be observable from a weathered tangential section (0.8 cm × 1.5 cm) of the eggshell of which the average diameter is 0.193 mm (Fig. 4B). The porosity of the *R. acicularis* would not be high given the rare distribution of pore canal in this section although it may not be a good representative of the density of pore canals considering the variation of pore density within an egg (Varricchio et al., 2013).

In radial view, the eggshell thickness ranges from 0.530 mm to 0.776 mm with an average of 0.649 mm. The eggshell consists of two layers: the inner mammillary and outer continuous layers (Fig. 4C–F). There is no external zone in *R. acicularis*. The fan-shaped to columnar extinction pattern is observed under polarized light (Fig. 4D, F) as in *Deinonychus* eggshell (Grellet-Tinner and Makovicky, 2006, fig. 1C).

In the mammillary layer, several eroded nucleation sites are observed, with some concave down arc-shaped structures, which are also observed from *Deinonychus* eggshell (Fig. 3B–C; Fig. 4C–D; Grellet-Tinner and Makovicky, 2006, fig. 1C). The needle-like acicular crystals are present in the mammillary layer but the center of radiation is not preserved in most mammillae (but see SEM image below). The acicular crystals radiate from the bases of mammillae and end at the inner horizontal growth lines of the continuous layer (Fig. 4E–F). The mammilla is wider than its height. The thickness of the mammillary layer ranges from 0.097 mm to 0.127 mm with an average of 0.109 mm. The boundary between the mammillary and continuous layers is clear-cut (abrupt) and similar to that of *Deinonychus* eggshell (Grellet-Tinner and Makovicky, 2006), *Paraelongatoolithus* (Wang et al., 2010), *Nipponoolithus* (Tanaka et al., 2016), and Elongatoolithidae (Huh et al., 2014; Pu et al., 2017; Tanaka et al., 2011; Zelenitsky and Therrien, 2008b; Zelenitsky et al., 2000) (Table 1). The continuous layer is characterized by lack of visible shell units, similar to 'ratite morphotype' (*sensu* Mikhailov, 1997a) eggshells (but see EBSD image below). The growth lines are clearly seen in the continuous layer, especially at the inner half of the layer. The similar trait was reported from *Deinonychus* eggshell, in which the density difference of growth lines is obvious (Grellet-Tinner and Makovicky, 2006). The growth lines are mainly parallel to each other, but they are slightly bent near the external pits as mentioned above (Fig. 4E–F). The thickness of the continuous layer ranges from 0.349 mm to 0.588 mm with an average of 0.474 mm. The ratio of the mammillary layer to the continuous layer is 1:2.2–1:2.6 with an average of 1:2.4.

SEM image. The mammillary layer is easily distinguished from the continuous layer in SEM images owing to their structural difference (Fig. 5). The calcite radial ultrastructure observed in the mammillary layer fans out externally from the nucleation center (Fig. 6A–B). In some cases, the crater-like structures (*sensu* Vila et al., 2017) are seen from where organic core existed. The acicular mammillae are morphologically very similar to those of the *Deinonychus* eggshell (Grellet-Tinner and Makovicky, 2006, fig. 2F; Zelenitsky, 2004, pl. 6.14) and *R. hirschi* (Zelenitsky and Sloboda, 2005). In a view from the radial-tangential orientation, the acicular structure shows "columnar jointing-like" shape with the polygonal cross section (Fig. 6C–D). At a high magnification (× 2000), the vesicles, known to be usually observed in the continuous layer (Mikhailov, 1997a), are also seen in the calcite radial ultrastructure (Fig. 6E). The acicular crystals appear to be partially oblique tabular sheet (Fig. 6E). The contact between the mammillary and continuous layers shows an abrupt change as seen in PLM images (Fig. 5). The squamatic ultrastructure occurs in the continuous layer (Fig. 5). The vertically stacked book-like structure is well developed in the inner half of the continuous layer (Fig. 6F). Many vesicles are seen in the various parts of the continuous layer. The continuous layer is morphologically homogeneous, which is different from *Prismatoolithus levis* that has an external zone (Funston and Currie, 2018; Jackson et al., 2010; Varricchio and Jackson, 2004).

EBSD image and misorientation distribution. The overall crystallographic features of *R. acicularis* are consistent with other maniraptoran eggshells in IPF maps (Fig. 7A, C; Choi et al., 2019). The mammillary layer is characterized by the acicular calcite radial ultrastructure, which can be unambiguously identified with the abundant low-angled (5°–10°) grain boundaries (Fig. 7B, D; Choi et al., 2019). The calcite grains in the mammillary layer are very narrow with a radiating arrangement. The mammillary layer is abruptly demarcated at the boundary between the mammillary and continuous layers in that the larger grains become predominant in the continuous layer. In the continuous layer, almost all calcite grains are aligned with their c-axis perpendicular to the eggshell surface. The continuous layer can be subdivided into two sublayers: the inner one-third of the continuous layer is composed of weakly prismatic calcite grains while the outer two-thirds one comprises highly irregular grains whose boundaries are highly rugged (Fig. 7B). The grains of the continuous layer are cryptoprismatic (at least in the inner sublayer) (*sensu* Jin et al., 2007) while prismatic grains do not extend to the end of the external surface unlike *Prismatoolithus levis* (Fig. 7B; Choi et al., 2019). In addition, the grain boundaries in the continuous layer are rugged, reflecting squamatic ultrastructure (Choi et al., 2019; Grellet-Tinner et al., 2012; López-Martínez and Vicens, 2012; Mikhailov, 1997b). Unlike oviraptorosaur eggshells, wave-like growth lines do not exist in the continuous layer. However, the low angle grain boundaries are widespread to the external surface along with the high angle boundaries, which are similar to the low angled grain boundary distribution of oviraptorosaur eggshells (Choi et al., 2019). As in *Elongatoolithus* sp., the external zone does not exist at the external end of the eggshell that can be supported by the absence of linear grain boundary (Choi et al., 2019). Several calcite grains of which c-axes parallel to the eggshell surface are observed near the external end of the eggshell (Fig. 7A). Considering the fact that some *R. acicularis* specimens may have been affected by diagenesis (see Taphonomic considerations above), these calcite grains with the horizontal c-axis would be the secondary calcite grains caused by recrystallization (Grellet-Tinner et al., 2012; Moreno-Azanza et al., 2013).

A possible pore canal was examined using EBSD analysis (Fig. 7C–D). It is located between the mammillae, where true pore

angle boundaries (green lines) in the mammillary and continuous layers. Squamatic ultrastructure is well represented by serrated grain boundaries in the continuous layer (Choi et al., 2019). The inner one-third of the continuous layer has rather prismatic and weakly rugged grain boundaries whereas outer two-thirds has strongly rugged grain boundaries. A dashed square is used for misorientation histogram in Fig. S1. (C) A possible pore canal (bounded by dashed lines). Note that calcite grains near this structure is weakly symmetrical in their c-axis orientation. (D) A possible pore canal is filled with calcites characterized by high-angle boundaries (white arrows). (E) Misorientation angle distribution is almost the same as those of oviraptorosaur and paleognath eggshells reported in Choi et al. (2019). Numbers in x- and y-axis are misorientation angles (degree) and probability, respectively. Blue bars are misorientation distribution under neighbor-pair method, whereas red bars random-pair one. The numbers next to each color index are sample sizes of neighbor-pair and random-pair distribution, respectively. All scale bars in A–D represent 250 μm.

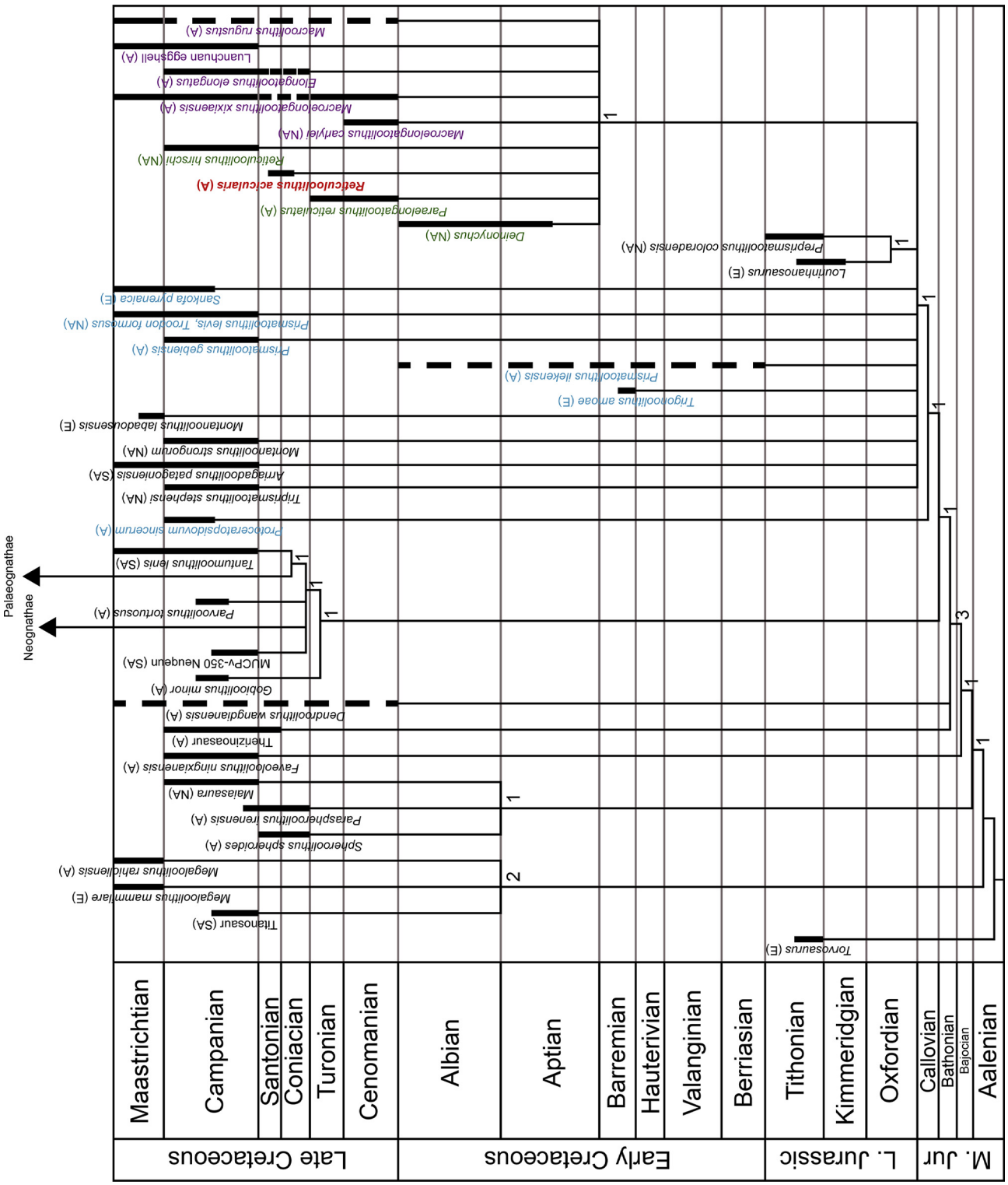
Late Cretaceous
Early Cretaceous
L. Jurassic
M. Jur
Maastrichtian
Campanian
Santonian
Coniacian
Turonian
Cenomanian
Albian
Aptian
Barremian
Hauterivian
Valanginian
Berriasian
Tithonian
Kimmeridgian
Oxfordian
Callovian
Bathonian
Bajocian
Aalenian
Palaeognathae
Neognathae
Torvosaurus (E)
Titanosaur (SA)
Megaloolithus mammillare (E)
Megaloolithus rahiolensis (A)
Spheroolithus spheroides (A)
Parasphaeroolithus irenensis (A)
Maiasaura (NA)
Faveoloolithus ningxianensis (A)
Therizinosaur (A)
Dendroolithus wangdianensis (A)
Gobioolithus minor (A)
MLCPv-350 Neuquen (SA)
Paroolithus tortuosus (A)
Tantumoolithus lenis (SA)
Protoceratopsidovum sincerum (A)
Triprismatoolithus stephensi (NA)
Arrugadoolithus patagoniensis (SA)
Montanoolithus strongorum (NA)
Montanoolithus labadousensis (E)
Prismatoolithus gebiensis (A)
Prismatoolithus levis, Troodon formosus (NA)
Sankofa pyrenaica (E)
Deinonychus (NA)
Paraelongatoolithus reticulatus (A)
Retiocuoolithus aciculatis (A)
Reticuloolithus hirschi (NA)
Macroelongatoolithus carlylei (NA)
Macroelongatoolithus xixiaensis (A)
Elongatoolithus elongatus (A)
Luanchuan eggshell (A)
Macroolithus rugustus (A)
Trigonoolithus amoae (E)
Prismatoolithus ilekensis (A)
Lourinhanosaurus (E)
Preprismatoolithus coloradensis (NA)
1
2
3

canals are formed (Tullett, 1975). In addition, the c-axis orientation of calcite grains beside the canal is not continuous to the opposite part of the canal (Choi et al., 2019). Because the c-axis orientation of calcite grains maintain continuity surrounding a crack (Fig. 3C), the canal shown in Figure 7 is a true pore canal. Although not perfectly preserved, the pore system would be angusticanaliculate or obliquicanaliculate consisting of tubular pores with the consistent width of openings on the outer and inner surfaces (Fig. 3A; Fig. 7C). Nevertheless, the angle of pore canals in *R. acicularis* is less steep than that of the typical obliquicanaliculate pore canals (e.g. Agnolin et al., 2012, fig. 10D; Antunes et al., 1998, fig. 6; Hirsch, 1994, fig. 10.3E) so that *R. acicularis* would be better described as having angusticanaliculate pore canals (Jin et al., 2007; Jackson et al., 2010). The pore canal is filled with randomly oriented calcite grains (characterized by the high angle grain boundaries), which are truly diagenetic in origin (Fig. 7D; Grellet-Tinner, 2005, fig. 4A; Grellet-Tinner et al., 2012; Kim et al., 2019; Moreno-Azanza et al., 2016).

A misorientation histogram was constructed using grain boundary angles (Fig. 7E). The neighbor-pair misorientation distribution belongs to Type 1 (*sensu* Choi et al., 2019) because a calculated value of d (see Choi et al., 2019 for further information) was 12.44 (Table S2). It is well matched with reported d values of oviraptorosaurs and paleognaths eggshells that have Type 1 misorientation distribution (Choi et al., 2019).

We further constructed a misorientation histogram from two mammillae, which confirms that lower angles are predominant (Fig. S1A; Table S3). Their misorientation distribution under neighbor-pair method showed that the average, median, and skewness are consistent with that of the acicular mammillary layer of oviraptorosaur eggshells. The ruggedness of two sublayers was further examined following the method of Choi et al. (2019). The result showed that there is a clear difference in ruggedness between two sublayers (Fig. S1B; Table S4).

5. Comparisons to putative dromaeosaurid eggshells

It should be noted that *R. acicularis* shows more remarkable similarity with *R. hirschi*, *Deinonychus* eggshell, *Paraelongatoolithus reticulatus*, and *Nipponoolithus ramosus* than other maniraptoran eggshells (Table 1). *R. acicularis* bears considerable resemblance to the Elongatoolithidae but there are several clear differences between them with ornamentation pattern and growth lines. It is apparent that *Reticuloolithus* does not belong to the Montanoolithidae and Prismatoolithidae because some of their diagnostic characters do not appear in *Reticuloolithus*.

Among maniraptoran egg fossils, *R. acicularis* is very similar to *Deinonychus* eggshell in following characters: the fan-shaped and acicular mammillary layer, abrupt boundary between the mammillary and continuous layers, ratio of the mammillary layer to the continuous layer, and non-undulating growth lines in the continuous layer (Grellet-Tinner and Makovicky, 2006). However, *R. acicularis* is thicker than *Deinonychus* eggshell (649 μm and 440 μm on average, respectively). In addition, the surface ornamentation looks more conspicuous in the *Deinonychus* eggshell although this difference may be originated from the poor preservation of *R. acicularis*. Hence, the only major difference between two types of eggs is the eggshell thickness, thereby they may be assignable to different oospecies within a single oogenus (Mikhailov et al., 1996; Hirsch et al., 1997). Because the same egg can have different thickness *per se* (Hirsch et al., 1997; Jin et al., 2007; Funston and Currie, 2018), however, the thickness variation between the *Deinonychus* eggshell and *R. acicularis* could be smaller than currently known. Unfortunately, *Deinonychus* eggshell has not yet been assigned to a parataxonomic nomenclature (Grellet-Tinner and Makovicky, 2006).

Paraelongatoolithus reticulatus was excavated from the Upper Cretaceous Chichengshan Formation in the Tiantai Basin, China, which is also very similar to *Reticuloolithus* (Wang et al., 2010). Both ootaxa have fan-shaped mammillary layer, the abrupt boundary between two layers, reticular ornamentation, and a similar ratio of the mammillary layer to the continuous layer. However, the mammillary layer of *P. reticulatus* seems to have weak acicular structure compared to that of *Reticuloolithus* and *Deinonychus* eggshell. Some ambiguous character states of the mammillary layer of *Paraelongatoolithus* could be identified in the near future with the quantitative approach via EBSD analysis. If *Paraelongatoolithus* has a definite acicular mammillary layer like *Reticuloolithus*, *Paraelongatoolithus* could be synonymized with oogenus *Reticuloolithus*. Until the character state of the mammillary layer is clearly identified in *Paraelongatoolithus reticulatus*, we regard *Paraelongatoolithus* as distinct oogenus.

Nipponoolithus ramosus from the Lower Cretaceous Sasayama Group in Japan (Tanaka et al., 2016) also shares similarity with *Reticuloolithus*: the abrupt boundary between two layers, irregular and blocky extinction pattern, and a similar ratio of the mammillary layer to the continuous layer. However, *R. acicularis* is about 1.5 times thicker than *Nipponoolithus*, and the mammillary layer of *Nipponoolithus* is ambiguous between acicular and wedge-like (Tanaka et al., 2016) as in *Paraelongatoolithus*. In addition, its linear branching ornamentation pattern appears to be different from those of *Reticuloolithus* and *Deinonychus* eggshells of which ornamentation are net-like (Zelenitsky and Sloboda, 2005; Grellet-Tinner and Makovicky, 2006).

The Elongatoolithidae shows strong similarity with *Reticuloolithus* such as a definite acicular mammillary layer confirmed by EBSD analysis and Type 1 misorientation angle distribution (Choi et al., 2019). In addition, EBSD images of *R. acicularis* show that both ooclades have a continuous layer with 'cryptic' prismatic calcite grains along with abundant low-angle grain boundaries (Fig. 7). However, *Reticuloolithus* does not show undulating growth

Fig. 8. The strict consensus tree of ootaxa plotted on a geological timescale (drawn to timescale). *Reticuloolithus acicularis* oosp. nov. is colored red, putative dromaeosaurid eggshells green, elongatoolithid eggshells purple, and prismatoolithid eggshells blue. Note that branching points on this cladogram do not reflect the cladogenetic events but just reflect the hypothetical phylogenetic relationship among the in-group ootaxa. The solid lines represent the temporal range of each ootaxon whereas the dotted lines represent the poor age resolution or uncertainty. Not all elongatoolithid analyzed is represented in the current cladogram due to the space, but all elongatoolithid is clustered within a node. Acronyms in parenthesis: A, Asia; E, Europe; NA, North America; SA, South America. The number at the braches are Bremer support vales. Temporal ranges are based on *Torvosaurus* (Araújo et al., 2013), titanosaur (Dingus et al., 2000), *Megaloolithus mammilare* (Fondevilla et al., 2016, 2019), *Megaloolithus rahioliensis* (Khosla et al., 2015), *Spheroolithus spheroids* (Zhao et al., 2013), *Paraspheroolithus irenensis* (Zhao et al., 2013), *Maiasaura* (Foreman et al., 2008), *Faveoloolithus ningxianensis* (Kim et al., 2008a), therizinosaur (Kundrát et al., 2008), *Dendroolithus wangdianensis* (Zhao and Li, 1988), *Triprismatoolithus stephensi* (Foreman et al., 2008), *Arriagadoolithus patagoniensis* (Agnolin et al., 2012), *Montanoolithus strongorum* (Eberth, 2005; Foreman et al., 2008), *Montanoolithus labadousensis* (Vila et al., 2017), *Trigonoolithus amoae* (Moreno-Azanza et al., 2014b), *Prismatoolithus ilekensis* (Skutschas et al., 2019), *Prismatoolithus gebiensis* (Eberth, 1993), *Prismatoolithus levis* (Zelenitsky and Hills, 1996; Varricchio and Jackson, 2004; Funston and Currie, 2018), *Sankofa pyrenaica* (López-Martínez and Vicens, 2012), *Protoceratopsidovum sincerum* (Dashzeveg et al., 2005), *Lourinhanosaurus* (Araújo et al., 2013; Ribeiro et al., 2014), *Preprismatoolithus coloradensis* (Maidment et al., 2017), *Gobioolithus minor* (Gradziński et al., 1977), MPCPv-350 (Dingus et al., 2000; Schweitzer et al., 2002), *Parvoolithus tortuosus* (Gradziński et al., 1977), *Tantumoolithus lenis* (Fernández and Salgado, 2018), *Deinonychus* (Oreska et al., 2013), *Paraelongatoolithus reticulatus* (Wang et al., 2010), *Reticuloolithus hirschi* (Eberth, 2005; Foreman et al., 2008), *Macroelongatoolithus carlylei* (Garrison Jr. et al., 2007), *Macroelongatoolithus xixiaensis* (Huh et al., 2014), *Elongatoolithus elongatus* (Zhao et al., 2013), Luanchuan eggshell (Tanaka et al., 2011), and *Macroolithus rugustus* (Zhao et al., 2002). General reference for the age of Late Cretaceous North American deposits: Fowler (2017).

lines nor linear ornamentation, which are diagnostic characters of the Elongatoolithidae (Carpenter, 1999). Moreover, the cryptoprismatic structure of *R. acicularis* appears only in the inner sublayer (Fig. 7) unlike that of *Macroelongatoolithus*, which is characterized by fully developed cryptoprismatic structure (Choi et al., 2019).

The oogenus *Montanoolithus* is composed of two oospecies from North America and Europe (Zelenitsky and Therrien, 2008a; Vila et al., 2017; Zelenitsky et al., 2017a; Voris et al., 2018). The overall morphology of *Montanoolithus* is similar to *Reticuloolithus*, especially the non-undulating horizontal growth lines in the continuous layer. However, both *Montanoolithus* oospecies are thicker than *Reticuloolithus*. In addition, the boundary between the mammillary and continuous layers of *Montanoolithus* is gradual unlike abrupt boundary of *R. acicularis*. Mammillary layer of *Montanoolithus* is wedge-like, not acicular as in *Reticuloolithus*. Finally, they have visible prismatic shell units in the continuous layer (Vila et al., 2017) whereas *R. acicularis* has cryptic (semi-) prismatic shell unit. Therefore, *Montanoolithus* is morphologically quite different from *Reticuloolithus*. *Reticuloolithus* does not belong to the Prismatoolithidae because it lacks gradual boundary condition and visible prismatic shell units (Moreno-Azanza et al., 2014b).

6. Phylogenetic analysis

We adopted the data matrix of Fernández and Salgado (2018) because it covered the most diverse ootaxa of theropod dinosaurs. We also critically reviewed and revised the data matrix according to the discussion of Whitlock et al. (2011). The resultant modifications are shown in Appendix 1 for a revised character matrix (see appendices of Tanaka et al., 2011 for original characters and their states). With *R. acicularis*, a total of 40 different eggshells and 16 characters were included in this phylogenetic analysis (Appendix 2).

A new phylogenetic analysis applied with the modifications shows that *R. acicularis* forms a monophyletic clade with *Deinonychus* eggshell, *R. hirschi*, *P. reticulatus*, and the Elongatoolithidae (Fig. 8).

Compared to the most recent cladogram (Fernández and Salgado, 2018), our revised matrix and its phylogenetic tree made several notable differences. First, the putative dromaeosaurid eggs and elongatoolithids showed a polytomic relationship in a single node. It may be caused by the unknown characters (see also Gerber, 2019 for effects of missing data) on the egg shape and clutch structure of putative dromaeosaurid ootaxa. If the two-sublayered continuous layer of *Deinonychus* eggshell and *Reticuloolithus acicularis* is confirmed to be a homology, and cryptoprismatic crystallography of *R. acicularis* is also observed in *Deinonychus* eggshell, *Paraelongatoolithus* or *Nipponoolithus*, we may distinguish putative dromaeosaurid eggs from the Elongatoolithidae with this diagnostic character.

Secondly, Tanaka et al., (2018) excluded *Preprismatoolithus* (basal allosauroid ootaxon; Carrano et al., 2013; M. Carrano pers. comm. 2017; Ribeiro et al., 2014) from the Prismatoolithidae and defined the Prismatoolithidae as a group solely composed of *Troodon* eggshell-like non-oviraptorosaur maniraptoran ootaxa. However, our revised cladogram still shows that *Preprismatoolithus* is more similar to other Cretaceous prismatoolithids than contemporary *Torvosaurus* eggshell at least in their morphology. This issue raises an intriguing question: why are basal allosauroid and maniraptoran eggshells similar in shape? If the typical microstructure of maniraptoran eggshells composed of the mammillary and continuous layers is a homology with that of basal allosauroid ones, we can say that the microstructure of avian eggshells dates back to the Late Jurassic. If a homoplasy, further clarification is needed as to why the microstructural differentiation that caused two-layers of eggshell independently occurred in basal allosauroid eggshells as well as derived maniraptoran eggshells.

On the other hand, because *Torvosaurus* and the egg-layers of *Preprismatoolithus* (i.e. *Lourinhanosaurus* and *Allosaurus*) are all basal tetanurans that temporally co-existed in the Late Jurassic and not highly distant phylogenetically (Carrano et al., 2012; Malafaia et al., 2017), some similarities in their eggshells may be homologies such as the oblique pore canal in both ootaxa (Hirsch, 1994; Araújo et al., 2013; Ribeiro et al., 2014), the pore lip of *Preprismatoolithus* (Hirsch, 1994) and sharp ridges on the outer surface of *Torvosaurus* eggshells (Araújo et al., 2013). Interestingly, *Arriagadoolithus* is the only Cretaceous ootaxon that possesses all these features (Agnolin et al., 2012). Investigating whether these similarities share 'common development' (*sensu* Hall, 2003, 2007) mechanism would be helpful to further test their possible homologous relationships (e.g. Choi et al., 2018).

Thirdly, our new cladogram yielded *Tantumoolithus* as a sister ootaxon of paleognath eggs. Among the confirmed or possible avian eggshells in this cladogram, *Tantumoolithus* is characterized by the 'ratite morphotype' continuous layer. All known enantiornithine eggshells are characterized by prismatic shell units (Kurochkin et al., 2013; Mikhailov et al., 1996; Schweitzer et al., 2002; Varricchio and Barta, 2015; but needs to be further confirmed in IGM 100/2010 (Balanoff et al., 2008; Varricchio et al., 2015) and egg of *Gobipteryx minuta* (Elźanowski, 1981)), whereas the continuous layer of paleognath eggshells do not have clear prismatic shell units (Choi et al., 2019; Grellet-Tinner, 2006; Mikhailov, 1997b; Zelenitsky and Modesto, 2003). Even though some neognath eggshells have 'ratite morphotype' (Hirsch et al., 1997), 'ratite morphotype' is much dominant in paleognaths among the modern avian eggshells. Considering that the origin of paleognaths may date back to the Late Cretaceous (Yonezawa et al., 2017; Berv and Field, 2018; Field et al., 2018), the 'ratite morphotype' *Tantumoolithus* may have a paleognath affinity. A putative *Lithornis* (Paleogene paleognath; Yonezawa et al., 2017) eggshell also shows the non-prismatic continuous layer (Grellet-Tinner and Dyke, 2005), supporting the view of paleognath affinity to *Tantumoolithus*. Because only a few 'ratite morphotype' eggshells were included in our matrix, however, additional 'ratite morphotype' possible avian eggshells (e.g. *Porituberoolithus warnerensis*, *Dispersituberoolithus exilis*, *Subtiliolithus microtuberculatus*, *Subtiliolithus kachchhensis Laevisoolithus sochavai*, *Tristraguloolithus cracioides*, *et cetera*; Jackson and Varricchio, 2010; Mikhailov, 1991, 1997a; Prondvai et al., 2017; Vianey-Liaud et al., 1997; Zelenitsky et al., 1996) are needed to be coded by the original authorities for the test of this hypothesis.

7. Discussion

Type 1 distribution of *Reticuloolithus acicularis*

R. acicularis has definite Type 1 distribution. The misorientation angle distribution of maniraptoran eggshells would be used for inference of brooding behavior (Choi et al., 2019) because low angle grain boundaries are prone to breakage but high angle grain boundaries are good at weight-bearing, usually caused by body weight of incubating parents (Rodriguez-Navarro et al., 2002; Moreno-Azanza et al., 2013). According to the view of Choi et al. (2019), low-angle skewed misorientation distribution (Type 1 distribution) may mean that the egg-layer may not adopt 'tight sitting (*sensu* Grant, 1982; associated with direct heat transfer mediated by brooding patch)' in incubation. *R. acicularis* showed typical Type 1 distribution which is shown in oviraptorid (*Elongatoolithus* sp.), giant caenagnathid (*Macroelongatoolithus xixiaensis*), and paleognath (ostrich and rhea) eggshells.

Whether dromaeosaurids did adopt contact incubation is yet unknown because no egg clutch was found associated with a brooding adult (Varricchio and Jackson, 2016). If Type 1 misorientation is indeed a sign of non-tight sitting in incubation, therefore, the crystallographic results in this study would be another line of inference on the brooding behavior of dromaeosaurids.

Dromaeosaurid records in the Cretaceous Korean Peninsula

The existence of dromaeosaurids in the Korean Peninsula has been confirmed by body and trace fossils. A maniraptoran femur with dromaeosaurid features was reported from the Early Cretaceous Gugyedong Formation (Kim et al., 2005). In addition, three didactyl ichnospecies (*Dromaeosauripus hamanensis*, *Dromaeosauripus jinjuensis*, and *Dromaeosauriformipes rarus*) were reported from the Early Cretaceous (Albian) Haman and Jinju formations (Kim et al., 2008b, 2012a; Kim et al., 2012b, 2018; Lee et al., 2018b). The dromaeosaurid didactyl footprints were also reported from the Early Cretaceous deposits in China (Li et al., 2006; Xing et al., 2013, 2016). Specifically, well-preserved dromaeosaurid body fossils have been found in the Early Cretaceous Jehol Biota in northeastern China (Benton et al., 2008; Zhou et al., 2003; Xu and Qin, 2017 and references therein) as well as the Early Cretaceous Bayan Gobi Formation in Inner Mongolia, China (Pittman et al., 2015). A putative dromaeosaurid ootaxon *Nipponoolithus ramosus* was also excavated from the Early Cretaceous Sasayama Group of Japan (Tanaka et al., 2016). All of these reports imply that dromaeosaurids were widely distributed in the Early Cretaceous of East Asia. It is also notable that the estimated size of *R. acicularis* (75.7 mm × 32.1 mm; see tables in Tanaka et al., 2016) is well matched with small dromaeosaurids (usually represented by the Microraptoria such as *Microraptor zhaoianus*, *Microraptor gui*, and *Zhongjianosaurus yangi*; Xu and Qin, 2017; Xu et al., 2000, 2003) and its probable trace fossils in East Asia (Kim et al., 2018).

However, there is no report on dromaeosaurid body and footprint fossils in the Late Cretaceous deposit in Korea. Nevertheless, the Late Cretaceous dromaeosaurids are well known in China (*Linheraptor* from the Wulansuhai Formation; Xu et al., 2010, 2015; but see also Turner et al., 2012) and Mongolia (*Adasaurus* from the Nemegt Formation, *Velociraptor* and *Tsaagan* from the Djadokhta Formation, and *Achillobator giganticus* from the Bayanshiree Formation; Turner et al., 2012). It is evident that dromaeosaurids thrived in the Late Cretaceous of East Asia. Therefore, it is reasonable that *R. acicularis* would be an egg of a dromaeosaurid dinosaur, supported by the paleobiogeography of dromaeosaurids.

A modifier 'putative' should not be overlooked

Until now, *Deinonychus* partial egg is the most plausible dromeosaurid egg material because this eggshell was associated with *Deinonychus* gastralia (Grellet-Tinner and Makovicky, 2006). If it is actually dromaeosaurid eggshell, it is highly probable that *Reticuloolithus*, *Paraelongatoolithus*, and *Nipponoolithus* are also dromaeosaurid eggshells (Zelenitsky and Sloboda, 2005; Tanaka et al., 2016). It was claimed that *Montanoolithus* may have a dromaeosaurid affinity (Vila et al., 2017; Voris et al., 2018; Zelenitsky and Therrien, 2008a; Zelenitsky et al., 2017a, 2017b), but it is morphologically dissimilar to other putative dromaeosaurid eggshells (Table 1; Fig. 8). In addition, *Montanoolithus* shares several features with the Prismatoolithidae: the gradual boundary between the mammillary and continuous layers, wedge-like mammillary layer, and prismatic shell units. Thus, we suggest that *Montanoolithus* might be more closely related to troodontids than dromaeosaurids.

Nevertheless, we would like to emphasize that taxonomic affinity of all 'putative dromaeosaurid' eggshells need to be confirmed because their affinity is far from certain. No dromaeosaurid embryo *in ovo* has yet discovered. For example, a common association between the prismatoolithid eggs and hysilophodont body fossils, and erroneous identification of an embryo fossil as having ornithischian affinity (MOR 246-11; Horner and Weishampel, 1988) led to the earlier confusion (e.g. Hirsch and Quinn, 1990) in the taxonomic affinity of *Prismatoolithus levis* as *Troodon formosus* eggs (Horner and Weishampel, 1996; Varricchio et al., 2002). Likewise, an interpretation of *Bonapartenykus ultimus* (alvarezsaurid) as an egg layer of *Arriagadoolithus patagoniensis* (Agnolin et al., 2012) was criticized by Jackson et al. (2018) who showed a close association of a neoceratopsian body fossil and turtle eggs, implying the possibility of unrelated taxa-ootaxa association. In addition, although it is still debated, the taxonomic affinity of "*Genyornis* eggs" from the Pleistocene deposit in Australia clearly shows that the assignment of egg fossils to a specific clade is prone to error even for Quaternary egg fossils (Grellet-Tinner et al., 2016, 2017; Miller et al., 2017) unless an embryo *in ovo* is present. Finally, in the peculiar case of "Tuştea puzzle," hadrosauroid hatchlings were associated with megaloolithid eggs (Grigorescu, 2010, 2017; Grigorescu et al., 2010; Botfalvai et al., 2017) which have been usually interpreted as titanosaur eggs based on embryos *in ovo* (Chiappe et al., 1998, 2001; Grellet-Tinner et al., 2011). Although still debated whether the association is a simple taphonomic artifact ('Scenario 1 and 2' in Botfalvai et al. (2017); Hechenleitner et al., 2015; Sellés et al., 2014; Weishampel and Jianu, 2011) or not (Bravo and Gaete, 2015; Botfalvai et al., 2017; Grigorescu, 2017), we believe this issue can be solved using EBSD analysis applied to Tuştea megaloolithids. Because EBSD can detect different developmental mechanism of convergent evolution (Hall, 2003; Choi et al., 2018), if disapproved as a taphonomic artifact, the "Tuştea puzzle" would be another strong case that body-egg association is not always be a powerful evidence in taxonomic inference for fossil eggshells.

Therefore, even though it is highly probable that *Deinonychus* eggshell and *Reticuloolithus* could be dromaeosaurid eggshells, it is premature to come to final conclusion until the dromaeosaurid embryo *in ovo* is reported.

8. Conclusions

The possible dromaeosaurid ootaxon *Reticuloolithus acicularis* oosp. nov. is reported from the Late Cretaceous of South Korea. *R. acicularis* has a strong similarity to *Reticuloolithus hirschi* and *Deinonychus* eggshells with an acicular mammillary layer, cryptoprismatic shell units, and a ratio of the mammillary layer to the continuous layer. Based on a newly revised character matrix, a comprehensive phylogenetic tree was presented for theropod eggshells. *R. acicularis* and other putative dromaeosaurid eggshells make a monophyly with the Elongatoolithidae, reflecting morphological and crystallographic similarities between two ooclades. Although our interpretation on the association between *R. acicularis* and a dromaeosaurid is conditional due to the absence of dromaeosaurid embryo fossil *in ovo*, our results potentially provide additional insight into the reproductive paleobiology of dromaeosaurids.

Acknowledgments

We thank Kohei Tanaka (University of Tsukuba, Tsukuba, Japan), Vasco Ribeiro (Museu da Lourinhã, Lourinhã, Portugal), Matthew Carrano (Smithsonian Institution, Washington, USA), and an anonymous reviewer of the first version of this manuscript who

kindly gave helpful advice and/or afforded unpublished data for the previous version of this article. We also thank Daniel Barta and an anonymous reviewer for their constructive comments and suggestions which greatly improved the manuscript. Seokyoung Han and Jihyuk Kim (Seoul National University) helped to make the thin section, to manipulate SEM, and provided their equipment. Seol Ji Kim (Inter-University Research Facilities, SNU) helped us to get a CL image. We especially thank In Gul Hwang and Yong Sik Gihm (Korea Institute of Geoscience and Mineral Resources), and Euijun Park, Noe-Heon Kim, and Seongyeong Kim (Paleontological Laboratory, SNU) who assisted us in the field. Noe-Heon Kim translated some Chinese literatures. We acknowledge Willi Hennig Society for the use of TNT. This work was supported by the National Research Foundation of Korea [grant number: 2019R1A2B5B02070240] to Yuong-Nam Lee.

Supplementary data

Supplementary data to this article can be found online at https://doi.org/10.1016/j.cretres.2019.06.013.

References

Agnolin, F.L., Powell, J.E., Novas, F.E., Kundrát, M., 2012. New alvarezsaurid (Dinosauria, Theropoda) from uppermost Cretaceous of north-western Patagonia with associated eggs. Cretaceous Research 35, 33–56.
Amiot, R., Wang, X., Wang, S., Lécuyer, C., Mazin, J.-M., Mo, J., Flandrois, J.-P., Fourel, F., Wang, X., Xu, X., Zhang, Z., Zhou, Z., 2017. $\delta^{18}O$-derived incubation temperature of oviraptorosaur eggs. Palaeontology 60, 633–647.
Antunes, M.T., Taquet, P., Ribeiro, V., 1998. Upper Jurassic dinosaur and crocodile eggs from Paimogo nesting site. Memórias da Academia de Ciências de Lisboa 37, 83–99.
Araújo, R., Castanhinha, R., Martins, R.M.S., Mateus, O., Hendrickx, C., Beckmann, F., Schell, N., Alves, L.C., 2013. Filling the gaps of dinosaur eggshell phylogeny: Late Jurassic theropod clutch with embryos from Portugal. Scientific Reports 3, 1924.
Athanasiadou, D., Jiang, W., Goldbaum, D., Saleem, A., Basu, K., Pacella, M.S., Böhm, C.F., Chromik, R.R., Hincke, M.T., Rodríguez-Navarro, A.B., Vali, H., Wolf, S.E., Gray, J.J., Bui, K.H., McKee, M.D., 2018. Nanostructure, osteopontin, and mechanical properties of calcitic avian eggshell. Science Advances 4 eaar3219.
Balanoff, A.M., Norell, M.A., Grellet-Tinner, G., Lewin, M.R., 2008. Digital preparation of a probable neoceratopsian preserved within an egg, with comments on microstructural anatomy of ornithischian eggshells. Naturwissenschaften 95, 493–500.
Behrensmeyer, A.K., Kidwell, S.M., Gastaldo, R.A., 2000. Taphonomy and paleobiology. Paleobiology 26, 103–147.
Benton, M.J., Zhou, Z., Orr, P.J., Zhang, F., Kearns, S.L., 2008. The remarkable fossils from the Early Cretaceous Jehol Biota of China and how they have changed our knowledge of Mesozoic life. Proceedings of the Geologists' Association 119, 209–228.
Berv, J.S., Field, D.J., 2018. Genomic signature of an avian Lilliput Effect across the K-Pg extinction. Systematic Biology 67, 1–13.
Bravo, A.M., Gaete, R., 2015. Titanosaur eggshells from the Tremp Formation (Upper Cretaceous, Southern Pyrenees, Spain). Historical Biology 27, 1079–1089.
Botfalvai, G., Csiki-Sava, Z., Grigorescu, D., Vasile, Ş., 2017. Taphonomical and palaeoecological investigation of the Late Cretaceous (Maastrichtian) Tuştea vertebrate assemblage (Romania; Haţeg Basin) – insights into a unique dinosaur nesting locality. Palaeogeography, Palaeoclimatology, Palaeoecology 468, 228–262.
Brusatte, S.L., O'Connor, J.K., Jarvis, E.D., 2015. The origin and diversification of birds. Current Biology 25, R888–R898.
Carpenter, K., 1999. Eggs, nests, and baby dinosaurs: a look at dinosaur reproduction. Indiana University Press, Bloomington.
Carrano, M.T., Benson, R.B.J., Sampson, S.D., 2012. The phylogeny of Tetanurae (Dinosauria: Theropoda). Journal of Systematic Palaeontology 10, 211–300.
Carrano, M., Mateus, O., Mitchell, J., 2013. First definitive association between embryonic Allosaurus bones and Prismatoolithus eggs in the Morrison Formation (Upper Jurassic, Wyoming, USA), vol. 101. Society of Vertebrate Paleontology Meeting Program and Abstracts.
Cheng, Y.-N., Ji, Q., Wu, X.-C., Shan, H.-Y., 2008. Oviraptorosaurian eggs (Dinosauria) with embryonic skeletons discovered for the first time in China. Acta Geologica Sinica 82, 1089–1094.
Chiappe, L.M., Coria, R.A., Dingus, L., Jackson, F., Chinsamy, A., Fox, M., 1998. Sauropod dinosaur embryos from the Late Cretaceous of Patagonia. Nature 396, 258–261.
Chiappe, L.M., Salgado, L., Coria, R.A., 2001. Embryonic skulls of titanosaur sauropod dinosaurs. Science 293, 2444–2446.
Choi, S., Lee, Y.-N., 2017. A review of vertebrate body fossils from the Korean Peninsula and perspectives. Geosciences Journal 21, 867–889.
Choi, S., Han, S., Kim, N.-H., Lee, Y.-N., 2018. A comparative study of eggshells of Gekkota with morphological, chemical compositional and crystallographic approaches and its evolutionary implications. PLoS One 13 (6), e0199496.
Choi, S., Han, S., Lee, Y.-N., 2019. Electron backscatter diffraction (EBSD) analysis of maniraptoran eggshells with important implications for microstructural and taphonomic interpretations. Palaeontology. https://doi.org/10.1111/pala.12427.
Chough, S.K., 2013. Geology and sedimentology of the Korean Peninsula. Elsevier, London.
Chough, S.K., Kwon, S.-T., Ree, J.-H., Choi, D.K., 2000. Tectonic and sedimentary evolution of the Korean Peninsula: a review and new view. Earth-Science Reviews 52, 175–235.
Clark, J.M., Norell, M.A., Chiappe, L.M., 1999. An oviraptorid skeleton from the Late Cretaceous of Ukhaa Tolgod, Mongolia, preserved in an avianlike brooding position over an oviraptorid nest. American Museum Novitates 3265, 1–36.
Clayburn, J.K., Smith, D.L., Hayward, J.L., 2004. Taphonomic effects of pH and temperature on extant avian dinosaur eggshell. PALAIOS 19, 170–177.
Dashzeveg, D., Dingus, L., Loope, D.B., Swisher III, C.C., Dulam, T., Sweeney, M.R., 2005. New stratigraphic subdivision, depositional environment, and age estimate for the Upper Cretaceous Djadokhta Formation, southern Ulan Nur Basin, Mongolia. American Museum Novitates 3498, 1–31.
Dingus, L., Clarke, J., Scott, G.R., Swisher III, C.C., Chiappe, L.M., Coria, R.A., 2000. Stratigraphy and magnetostratigraphic/faunal constraints for the age of sauropod embryo-bearing rocks in the Neuquén Group (Late Cretaceous, Neuquén Province, Argentina). American Museum Novitates 3290, 1–11.
Eberth, D.A., 1993. Depositional environments and fades transitions of dinosaur-bearing Upper Cretaceous redbeds at Bayan Mandahu (Inner Mongolia, People's Republic of China). Canadian Journal of Earth Sciences 30, 2196–2213.
Eberth, D.A., 2005. The Geology (Chapter 3). In: Currie, P.J., Koppelhus, E.B. (Eds.), Dinosaur Provincial Park: a spectacular ancient ecosystem revealed. Indiana University Press, Bloomington, pp. 54–82.
Elźanowski, A., 1981. Embryonic bird skeletons from the Late Cretaceous of Mongolia. Palaeontologia Polonica 42, 147–179.
Fanti, F., Currie, P.J., Badamgarav, D., 2012. New specimens of *Nemegtomaia* from the Baruungoyot and Nemegt formations (Late Cretaceous) of Mongolia. PLoS One 7 (2), e31330.
Fernández, M.S., Salgado, L., 2018. The youngest egg of avian affinities from the Cretaceous of Patagonia. Historical Biology. https://doi.org/10.1080/08912963.2018.1470622.
Fowler, D.W., 2017. Revised geochronology, correlation, and dinosaur stratigraphic ranges of the Santonian–Maastrichtian (Late Cretaceous) formations of the Western Interior of North America. PLoS One 12 (11), e0188426.
Field, D.J., Bercovici, A., Berv, J.S., Dunn, R., Fastovsky, D.E., Lyson, T.R., Vajda, V., Gauthier, J.A., 2018. Early evolution of modern birds structured by global forest collapse at the end-Cretaceous mass extinction. Current Biology 28, 1825–1831.
Fondevilla, V., Dinarès-Turell, J., Vila, B., Le Loeuff, J., Estrada, R., Oms, O., Galobart, À., 2016. Magnetostratigraphy of the Maastrichtian continental record in the Upper Aude Valley (northern Pyrenees, France): Placing age constraints on the succession of dinosaur-bearing sites. Cretaceous Research 57, 457–472.
Fondevilla, V., Riera, V., Vila, B., Dinarès-Turell, J., Vicens, E., Gaete, R., Oms, O., Galobart, À., 2019. Chronostratigraphic synthesis of the latest Cretaceous dinosaur turnover in south-western Europe. Earth-Science Reviews 191, 168–189.
Foreman, B.Z., Rogers, R.R., Deino, A.L., Wirth, K.R., Thole, J.T., 2008. Geochemical characterization of bentonite beds in the Two Medicine Formation (Campanian, Montana), including a new $^{40}Ar/^{39}Ar$ age. Cretaceous Research 29, 373–385.
Funston, G.F., Currie, P.J., 2018. The first record of dinosaur eggshell from the Horseshoe Canyon Formation (Maastrichtian) of Alberta, Canada. Canadian Journal of Earth Sciences 55, 436–441.
Garcia, G., Feist, M., Cabot, A., Valentin, X., Vianey-Liaud, M., 2000. Les œufs de dinosaures du Crétacé supérieur du bassin de Villeveyrac-Méze (Hérault, France): description d'une nouvelle ooespéce de *Prismatoolithus*. Bulletin de la Societe Geologique de France 171, 283–289 (in French with English summary).
Garrison Jr., J.R., Brinkman, D., Nichols, D.J., Layer, P., Burge, D., Thayn, D., 2007. A multidisciplinary study of the Lower Cretaceous Cedar Mountain Formation, Mussentuchit Wash, Utah: a determination of the paleoenvironment and paleoecology of the *Eolambia caroljonesa* dinosaur quarry. Cretaceous Research 28, 461–494.
Gerber, S., 2019. Use and misuse of discrete character data for morphospace and disparity analyses. Palaeontology 62, 305–319. https://doi.org/10.1111/pala.12407.
Gihm, Y.S., Hwang, I.G., 2014. Syneruptive and intereruptive lithofacies in lacustrine environments: The Cretaceous Beolkeum Member, Wido Island, Korea. Journal of Volcanology and Geothermal Research 273, 15–32.
Gihm, Y.S., Hwang, I.G., 2016. Lacustrine hyperpycnal flow deposits after explosive volcanic eruptions, Cretaceous Beolkeum Member, Wido Island, Korea. Geosciences Journal 20, 157–166.
Gihm, Y.S., Kim, M.-C., Son, M., Hwang, I.G., 2017. The influence of tectonic subsidence on volcaniclastic sedimentation: The Cretaceous upper Daeri Member, Wido Island, Korea. Island Arc 26, e12183.

Goloboff, P.A., Catalano, S.A., 2016. TNT version 1.5, including a full implementation of phylogenetic morphometrics. Cladistics 32, 221–238.
Grant, G.S., 1982. Avian incubation: egg temperature, nest humidity, and behavioral thermoregulation in a hot environment. Ornithological Monographs 30, 1–75.
Grellet-Tinner, G., 2005. Membrana testacea of titanosaurid dinosaur eggs from Auca Mahuevo (Argentina): implications for exceptional preservation of soft tissue in Lagerstätten. Journal of Vertebrate Paleontology 25, 99–106.
Grellet-Tinner, G., 2006. Phylogenetic interpretation of eggs and eggshells: implications for phylogeny of Palaeognathae. Alcheringa: An Australasian Journal of Palaeontology 30, 141–182.
Grellet-Tinner, G., Dyke, G.J., 2005. The eggshell of the Eocene bird *Lithornis*. Acta Palaeontologica Polonica 50, 831–835.
Grellet-Tinner, G., Makovicky, P., 2006. A possible egg of the dromaeosaur *Deinonychus antirrhopus*: phylogenetic and biological implications. Canadian Journal of Earth Sciences 43, 705–719.
Grellet-Tinner, G., Corsetti, F., Buscalioni, A.D., 2010. The importance of microscopic examinations of eggshells: Discrimination of bioalteration and diagenetic overprints from biological features. Journal of Iberian Geology 36, 181–192.
Grellet-Tinner, G., Sim, C.M., Kim, D.H., Trimby, P., Higa, A., An, S.L., Oh, H.S., Kim, T.J., Kardjilov, N., 2011. Description of the first lithostrotian titanosaur embryo in ovo with Neutron characterization and implications for lithostrotian Aptian migration and dispersion. Gondwana Research 20, 621–629.
Grellet-Tinner, G., Murelaga, X., Larrasoaña, J.C., Silveira, L.F., Olivares, M., Ortega, L.A., Trimby, P.W., Pascual, A., 2012. The first occurrence in the fossil record of an aquatic avian twig-nest with Phoenicopteriformes eggs: evolutionary implications. PLoS One 7 (10), e46972.
Grellet-Tinner, G., Spooner, N.A., Worthy, T.H., 2016. Is the "*Genyornis*" egg of a mihirung or another extinct bird from the Australian dreamtime? Quaternary Science Reviews 133, 147–164.
Grellet-Tinner, G., Spooner, N.A., Worthy, T.H., 2017. The Genyornis egg: response to Miller et al.'s commentary on Grellet-Tinner et al, 2016. Quanternary Science Reviews 161, 128–133.
Grigorescu, D., 2010. The "Tustea Puzzle": hadrosaurid (Dinosauria, Ornithopoda) hatchlings associated with Megaloolithidae eggs in the Maastrichtian of the Hateg Basin (Romania). Ameghiniana 47, 89–97.
Grigorescu, D., 2017. The 'Tuştea puzzle' revisited: Late Cretaceous (Maastrichtian) *Megaloolithus* eggs associated with *Telmatosaurus* hatchlings in the Haţeg Basin. Historical Biology 29, 627–640.
Godefroit, P., Cau, A., Hu, D.-Y., Escuillié, F., Wu, W., Dyke, G., 2013. A Jurassic avialan dinosaur from China resolves the early phylogenetic history of birds. Nature 498, 359–362.
Gradziński, R., Kielan-Jaworowska, Z., Maryańska, T., 1977. Upper Cretaceous Djadokhta, Barun Goyot and Nemegt formations of Mongolia, including remarks on previous subdivisions. Acta Geologica Polonica 27, 281–318.
Grigorescu, D., Garcia, G., Csiki, Z., Codrea, V., Bojar, A.-V., 2010. Uppermost Cretaceous megaloolithid eggs from the Haţeg Basin, Romania, associated with hadrosaur hatchlings: Search for explanation. Palaeogeography, Palaeoclimatology, Palaeoecology 293, 360–374.
Hall, B.K., 2003. Descent with modification: the unity underlying homology and homoplasy as seen through an analysis of development and evolution. Biological Reviews 78, 409–433.
Hall, B.K., 2007. Homoplasy and homology: Dichotomy or continuum? Journal of Human Evolution 52, 473–479.
Hauber, M.E., 2014. The book of eggs: A lifesize guide to the eggs of six hundred of the world's bird species. The University of Chicago Press, Chicago.
Hechenleitner, E.M., Grellet-Tinner, G., Fiorelli, L.E., 2015. What do giant titanosaur dinosaurs and modern Australasian megapodes have in common? PeerJ 3, e1341.
Hirsch, K.F., 1994. Upper Jurassic eggshells from the Western Interior of North America (Chapter 10). In: Carpenter, K., Hirsch, K.F., Horner, J.R. (Eds.), Dinosaur eggs and babies. Cambridge University Press, New York, pp. 137–150.
Hirsch, K.F., Quinn, B., 1990. Eggs and eggshell fragments from the Upper Cretaceous Two Medicine Formation of Montana. Journal of Vertebrate Paleontology 10, 491–511.
Hirsch, K.F., Kihm, A.J., Zelenitsky, D.K., 1997. New eggshell of ratite morphotype with predation marks from the Eocene of Colorado. Journal of Vertebrate Paleontology 17, 360–369.
Horner, J.R., Weishampel, D.B., 1988. A comparative embryological study of two ornithischian dinosaurs. Nature 332, 256–257.
Horner, J.R., Weishampel, D.B., 1996. Correction - A comparative embryological study of two ornithischian dinosaurs. Nature 383, 103.
Huh, M., Paik, I.S., Park, J., Hwang, K.G., Lee, Y.I., Yang, S.Y., Lim, J.D., Lee, Y.U., Cheong, D.K., Seo, S.J., Park, K.H., Moon, K.H., 2006. Occurrence of dinosaur eggs in South Korea. Journal of the Geological Society of Korea 42, 523–547 (in Korean with English abstract).
Huh, M., Kim, B.S., Woo, Y., Simon, D.J., Paik, I.S., Kim, H.J., 2014. First record of a complete giant theropod egg clutch from Upper Cretaceous deposits, South Korea. Historical Biology 26, 218–228.
Jackson, F.D., Varricchio, D.J., 2010. Fossil eggs and eggshell from the lowermost Two Medicine Formation of western Montana, Sevenmile Hill locality. Journal of Vertebrate Paleontology 30, 1142–1156.
Jackson, F.D., Varricchio, D.J., 2016. Fossil egg and eggshells from the Upper Cretaceous Hell Creek Formation, Montana. Journal of Vertebrate Paleontology 36, e1185432. https://doi.org/10.1080/02724634.2016.1185432.
Jackson, F.D., Horner, J.R., Varricchio, D.J., 2010. A study of a *Troodon* egg containing embryonic remains using epifluorescence microscopy and other techniques. Cretaceous Research 31, 255–262.
Jackson, F.D., Schaff, R.J., Varricchio, D.J., Schmitt, J.G., 2015. A theropod nesting trace with eggs from the Upper Cretaceous (Campanian) Two Medicine Formation of Montana. PALAIOS 30, 362–372.
Jackson, F.D., Zheng, W., Imai, T., Jackson, R.A., Jin, X., 2018. Fossil eggs associated with a neoceratopsian (*Mosaiceratops azumai*) from the Upper Cretaceous Xiaguan Formation, Henan Province, China. Cretaceous Research 91, 457–467.
Jin, X., Azuma, Y., Jackson, F.D., Varricchio, D.J., 2007. Giant dinosaur eggs from the Tiantai basin, Zhejiang Province, China. Canadian Journal of Earth Sciences 44, 81–88.
Jin, X., Jackson, F.D., Varricchio, D.J., Azuma, Y., He, T., 2010. The first *Dictyoolithus* egg clutches from the Lishui Basin, Zhejiang Province, China. Journal of Vertebrate Paleontology 30, 188–195.
Karlsson, O., Lilja, C., 2008. Eggshell structure, mode of development and growth rate in birds. Zoology 111, 494–502.
Khosla, A., Chin, K., Alimohammadin, H., Dutta, D., 2015. Ostracods, plant tissues, and other inclusions in coprolites from the Late Cretaceous Lameta Formation at Pisdura, India: Taphonomical and palaeoecological implications. Palaeogeography, Palaeoclimatology, Palaeoecology 418, 90–100.
Kim, H.M., Gishlick, A.D., Tsuihiji, T., 2005. The first non-avian maniraptoran skeletal remains from the Lower Cretaceous of Korea. Cretaceous Research 26, 299–306.
Kim, C.-B., Kim, J., Huh, M., 2008a. Age and stratification of dinosaur eggs and clutches from Seonso Formation, South Korea. Journal of the Korean Earth Science Society 29, 386–395.
Kim, J.Y., Kim, K.S., Lockley, M.G., Yang, S.Y., Seo, S.J., Choi, H.I., Lim, J.D., 2008b. New didactyl dinosaur footprints (*Dromaeosauripus hamanensis* ichnogen. et ichnosp. nov.) from the Early Cretaceous Haman Formation, south coast of Korea. Palaeogeography, Palaeoclimatology, Palaeoecology 262, 72–78.
Kim, J.Y., Yang, S.Y., Choi, H.I., Seo, S.J., Kim, K.S., 2011. Dinosaur eggs from the Cretaceous Goseong Formation of Tongyeong City, southern coast of Korea. Journal of the Paleontological Society of Korea 27, 13–26.
Kim, J.Y., Lockley, M.G., Woo, J.O., Kim, S.H., 2012a. Unusual didactyl traces from the Jinju Formation (Early Cretaceous, South Korea) indicate a new ichnospecies of *Dromaeosauripus*. Ichnos 19, 75–83.
Kim, K.S., Lockley, M.G., Kim, J.Y., Seo, S.J., 2012b. The smallest dinosaur tracks in the world: occurrences and significance of *Minisauripus* from East Asia. Ichnos 19, 66–74.
Kim, K.S., Lim, J.D., Lockley, M.G., Xing, L., Kim, D.H., Piñuela, L., Romilio, A., Yoo, J.S., Kim, J.H., Ahn, J., 2018. Smallest known raptor tracks suggest microraptorine activity in lakeshore setting. Scientific Reports 8, 16908.
Kim, N.-H., Choi, S., Kim, S., Lee, Y.-N., 2019. A new faveoloolithid oogenus from the Wido Volcanics (Upper Cretaceous), South Korea and a new insight into the oofamily Faveoloolithidae. Cretaceous Research 100, 145–163.
Kim, S.W., Kwon, S., Park, S.-I., Lee, C., Cho, D.-L., Lee, H.-J., Ko, K., Kim, S.J., 2016. SHRIMP U-Pb dating and geochemistry of the Cretaceous plutonic rocks in the Korean Peninsula: A new tectonic model of the Cretaceous Korean Peninsula. Lithos 262, 88–106.
Ko, K., Kim, S.W., Lee, H.-J., Hwang, I.G., Kim, B.C., Kee, W.-S., Kim, Y.-S., Gihm, Y.S., 2017. Soft sediment deformation structures in a lacustrine sedimentary succession induced by volcano-tectonic activities: An example from the Cretaceous Beolgeumri Formation, Wido Volcanics, Korea. Sedimentary Geology 358, 197–209.
Koh, H.J., Kwon, C.W., Park, S.I., Park, J., Kee, W.-S., 2013. Geological report of the Julpo and Wido · Hawangdeungdo sheets (1: 50,000). Korea Institute of Geoscience and Mineral Resources, Daejeon (in Korean with English summary).
Kundrát, M., Cruickshank, A.R.I., Manning, T.W., Nudds, J., 2008. Embryos of therizinosauroid theropods from the Upper Cretaceous of China: diagnosis and analysis of ossification patterns. Acta Zoologica 89, 231–251.
Kurochkin, E.N., Chatterjee, S., Mikhailov, K.E., 2013. An embryonic enantinornithine bird and associated eggs from the Cretaceous of Mongolia. Paleontological Journal 47, 1252–1269.
Kwon, C.W., Ko, K., Gihm, Y.S., Koh, H.J., Kim, H., 2017. Late Cretaceous volcanic arc system in southwest Korea: Distribution, lithology, age, and tectonic implications. Cretaceous Research 75, 125–140.
Lee, T.-H., Park, K.-H., Yi, K., 2018a. SHRIMP U-Pb ages of detrital zircons from the Early Cretaceous Nakdong Formation, South East Korea: Timing of initiation of the Gyeongsang Basin and its provenance. Island Arc 27, e12258.
Lee, T.-H., Park, K.-H., Yi, K., 2018b. Nature and evolution of the Cretaceous basins in the eastern margin of Eurasia: A case study of the Gyeongsang Basin, SE Korea. Journal of Asian Earth Sciences 166, 19–31.
Lee, Y.-N., 2003. Dinosaur bones and eggs in South Korea. Memoir of the Fukui Prefectural Dinosaur Museum 2, 113–121.
Lee, Y.-N., 2017. Dinosaur eggs and nests in South Korea and their contributions to dinosaur research and conservation. Proceedings and Field Guidebook for the Fifth International Symposium of International Geoscience Programme IGCP Project 608, 9.
Lee, Y.-N., Yu, K.-M., Wood, C.B., 2001. A review of vertebrate faunas from the Gyeongsang Supergroup (Cretaceous) in South Korea. Palaeogeography, Palaeoclimatology, Palaeoecology 165, 357–373.
Lee, Y.-N., Kim, B.C., Lee, Y.S., Kee, W.-S., 2007. New dinosaur eggsite found in the Namyang Basin, Hwaseong City, Gyeonggi Province. Journal of the Paleontological Society of Korea 23, 15–26 (in Korean with English abstract).
Lee, Y.U., 2008. Dinosaur skeletons from the Cretaceous Gurye Basin, Jellanam-do, Korea. Journal of the Geological Society of Korea 44, 353–357 (in Korean).

Li, D., Azuma, Y., Fujita, M., Lee, Y.-N., Arakawa, Y., 2006. A preliminary report on two new vertebrate track sites including dinosaurs from the Early Cretaceous Hekou Group, Gansu Province, China. Journal of the Paleontological Society of Korea 22, 29–49.
López-Martínez, N., Vicens, E., 2012. A new peculiar dinosaur egg, *Sankofa pyrenaica* oogen. nov. oosp. nov. from the Upper Cretaceous coastal deposits of the Aren Formation, south-central Pyrenees, Lleida, Catalonia, Spain. Palaeontology 55, 325–339.
Machel, H.G., 1985. Cathodoluminescence in calcite and dolomite and its chemical interpretation. Geoscience Canada 12, 139–147.
Maidment, S.C.R., Balikova, D., Muxworthy, A.R., 2017. Magnetostratigraphy of the Upper Jurassic Morrison Formation at Dinosaur National Monument, Utah, and prospects for using magnetostratigraphy as a correlative tool in the Morrison Formation. In: Zeigler, K.E., Parker, W.G. (Eds.), Terrestrial depositional systems: Deciphering complexities through multiple stratigraphic methods. Elsevier, pp. 279–302.
Malafaia, E., Mocho, P., Escaso, E., Ortega, F., 2017. A juvenile allosauroid theropod (Dinosauria, Saurischia) from the Upper Jurassic of Portugal. Historical Biology 29, 654–676.
Mikhailov, K.E., 1991. Classification of fossil eggshells of amniotic vertebrates. Acta Palaeontologica Polonica 36, 193–238.
Mikhailov, K.E., 1994. Theropod and protoceratopsian dinosaur eggs from the Cretaceous of Mongolia and Kazakhstan. Paleontological Journal 28, 101–120.
Mikhailov, K.E., 1997a. Fossil and recent eggshell in amniotic vertebrates: fine structure, comparative morphology and classification. Special Papers in Palaeontology 56, 1–80.
Mikhailov, K.E., 1997b. Avian eggshells: an atlas of scanning electron micrographs. British Ornithologists Club Occasional Publications 3, 1–88.
Mikhailov, K.E., 2014. Eggshell structure, parataxonomy and phylogenetic analysis: some notes on articles published from 2002 to 2011. Historical Biology 26, 144–154.
Mikhailov, K.E., Bray, E.S., Hirsch, K.F., 1996. Parataxonomy of fossil egg remains (Verterovata): principles and applications. Journal of Vertebrate Paleontology 16, 763–769.
Miller, G.H., Fogel, M.L., Magee, J.W., Clarke, S.J., 2017. The *Genyornis* egg: A commentary on Grellet-Tinner et al., 2016. Quaternary Science Reviews 161, 123–127.
Moreno-Azanza, M., Mariani, E., Bauluz, B., Canudo, J.I., 2013. Growth mechanisms in dinosaur eggshells: an insight from electron backscatter diffraction. Journal of Vertebrate Paleontology 33, 121–130.
Moreno-Azanza, M., Canudo, J.I., Gasca, J.M., 2014a. Spheroolithid eggshells in the Lower Cretaceous of Europe. Implications for eggshell evolution in ornithischian dinosaurs. Cretaceous Research 51, 75–87.
Moreno-Azanza, M., Canudo, J.I., Gasca, J.M., 2014b. Unusual theropod eggshells from the Early Cretaceous Blesa Formation of the Iberian Range, Spain. Acta Palaeontologica Polonica 59, 843–854.
Moreno-Azanza, M., Bauluz, B., Canudo, J.I., Gasca, J.M., Fernández-Baldor, F.T., 2016. Combined use of electron and light microscopy techniques reveals false secondary shell units in Megaloolithidae eggshells. PLoS One 11 (5), e0153026.
Moreno-Azanza, M., Bauluz, B., Canudo, J.I., Mateus, O., 2017. The conservative structure of the ornithopod eggshell: electron backscatter diffraction characterization of *Guegoolithus turolensis* from the Early Cretaceous of Spain. Journal of Iberian Geology 43, 235–243.
Norell, M.A., Clark, J.M., Chiappe, L.M., Dashzeveg, D., 1995. A nesting dinosaur. Nature 378, 774–776.
Norell, M.A., Clark, J.M., Chiappe, L.M., 2001. An embryonic oviraptorid (Dinosauria: Theropoda) from the Upper Cretaceous of Mongolia. American Museum Novitates 3315, 1–17.
Norell, M.A., Balanoff, A.M., Barta, D.E., Erickson, G.M., 2018. A second specimen of *Citipati osmolskae* associated with a nest of eggs from Ukhaa Tolgod, Omnogov Aimag, Mongolia. American Museum Novitates 3899, 1–44.
Oreska, M.P.J., Carrano, M.T., Kzikiewicz, K.M., 2013. Vertebrate paleontology of the Cloverly Formation (Lower Cretaceous), I: Faunal composition, biogeographic relationships, and sampling. Journal of Vertebrate Paleontology 33, 264–292.
Paik, I.S., Huh, M., Kim, H.J., 2004. Dinosaur egg-bearing deposits (Upper Cretaceous) of Boseong, Korea: occurrence, palaeoenvironments, taphonomy, and preservation. Palaeogeography, Palaeoclimatology, Palaeoecology 205, 155–168.
Paik, I.S., Kim, H.J., Huh, M., 2012. Dinosaur egg deposits in the Cretaceous Gyeongsang Supergroup, Korea: Diversity and paleobiological implications. Journal of Asian Earth Sciences 56, 135–146.
Pittman, M., Pei, R., Tan, Q., Xu, X., 2015. The first dromaeosaurid (Dinosauria: Theropoda) from the Lower Cretaceous Bayan Gobi Formation of Nei Mongol, China. PeerJ 3, e1480.
Prondvai, E., Botfalvai, G., Stein, K., Szentesi, Z., Ősi, A., 2017. Collection of the thinnest: A unique eggshell assemblage from the Late Cretaceous vertebrate locality of Iharkút (Hungary). Central European Geology 60, 73–133.
Pu, H., Zelenitsky, D.K., Lü, J., Currie, P.J., Carpenter, K., Xu, L., Koppelhus, E.B., Jia, S., Xiao, L., Chuang, H., Li, T., Kundrát, M., Shen, C., 2017. Perinate and eggs of a giant caenagnathid dinosaur from the Late Cretaceous of central China. Nature Communications 8, 14952.
Quinn, B., 1994. Fossilized eggshell preparation (Chapter 6). In: Leiggi, P., May, P. (Eds.), Vertebrate paleontological techniques, vol. 1. Cambridge University Press, New York, pp. 146–153.
Ribeiro, V., Mateus, O., Holwerda, F., Araújo, R., Castanhinha, R., 2014. Two new theropod egg sites from the Late Jurassic Lourinhã Formation, Portugal. Historical Biology 26, 206–217.
Rodriguez-Navarro, A., Kalin, O., Nys, Y., Garcia-Ruiz, J.M., 2002. Influence of the microstructure on the shell strength of eggs laid by hens of different age. British Poultry Science 43, 395–403.
Ryu, I.-C., Lee, C., 2017. Intracontinental mantle plume and its implications for the Cretaceous tectonic history of East Asia. Earth and Planetary Science Letters 479, 206–218.
Sellés, A.G., Vila, B., Galobart, À., 2014. *Spheroolithus europaeus*, oosp. nov. (Late Maastrichtian, Catalonia), the youngest oological record of hadrosauroids in Eurasia. Journal of Vertebrate Paleontology 34, 725–729.
Sereno, P.C., 1997. The origin and evolution of dinosaurs. Annual Review of Earth and Planetary Sciences 25, 435–489.
Sato, T., Cheng, Y.-N., Wu, X.-C., Zelenitsky, D.K., Hsiao, Y.-F., 2005. A pair of shelled eggs inside a female dinosaur. Science 308, 375.
Schweitzer, M.H., Jackson, F.D., Chiappe, L.M., Schmitt, J.G., Calvo, J.O., Rubilar, D.E., 2002. Late Cretaceous avian eggs with embryos from Argentina. Journal of Vertebrate Paleontology 22, 191–195.
Skutschas, P.P., Markova, V.D., Boitsova, E.A., Leshchinskiy, S.V., Ivantsov, S.V., Maschenko, E.N., Averianov, A.O., 2019. The first dinosaur egg from the Lower Cretaceous of Western Siberia, Russia. Historical Biology 31, 836–844. https://doi.org/10.1080/08912963.2017.1396322.
Smith, D.L., Hayward, J.L., 2010. Bacterial decomposition of avian eggshell: A taphonomic experiment. PALAIOS 25, 318–326.
Stein, K., Prondvai, E., Huang, T., Baele, J.-M., Sander, P.M., Reisz, R., 2019. Structure and evolutionary implications of the earliest (Sinemurian, Early Jurassic) dinosaur eggs and eggshells. Scientific Reports 9, 4424.
Tanaka, K., Lü, J., Kobayashi, Y., Zelenitsky, D.K., Xu, L., Jia, S., Qin, S., Tang, M., 2011. Description and phylogenetic position of dinosaur eggshells from the Luanchuan area of western Henan Province, China. Acta Geologica Sinica (English Edition) 85, 66–74.
Tanaka, K., Zelenitsky, D.K., Saegusa, H., Ikeda, T., DeBuhr, C.L., Therrien, F., 2016. Dinosaur eggshell assemblage from Japan reveals unknown diversity of small theropods. Cretaceous Research 57, 350–363.
Tanaka, K., Zelenitksy, D.K., Therrien, F., Kobayashi, Y., 2018. Nest substrate reflects incubation style in extant archosaurs with implications for dinosaur nesting habits. Scientific Reports 8, 3170.
Tullett, S.G., 1975. Regulation of avian eggshell porosity. Journal of Zoology 177, 339–348.
Turner, A.H., Makovicky, P.J., Norell, M.A., 2012. A review of dromaeosaurid systematics and paravian phylogeny. Bulletin of the American Museum of Natural History 371, 1–206.
van der Reest, A.J., Currie, P.J., 2017. Troodontids (Theropoda) from the Dinosaur Park Formation, Alberta, with a description of a unique new taxon: implications for deinonychosaur diversity in North America. Canadian Journal of Earth Sciences 54, 919–935.
Varricchio, D.J., Barta, D.E., 2015. Revisiting Sabath's "Larger Avian Eggs" from the Gobi Cretaceous. Acta Palaeontologica Polonica 60, 11–25.
Varricchio, D.J., Jackson, F.D., 2004. A phylogenetic assessment of prismatic dinosaur eggs from the Cretaceous Two Medicine Formation of Montana. Journal of Vertebrate Paleontology 24, 931–937.
Varricchio, D.J., Jackson, F.D., 2016. Reproduction in Mesozoic birds and evolution of the modern avian reproductive mode. The Auk: Ornithological Advances 133, 654–684.
Varricchio, D.J., Jackson, F., Borkowski, J.J., Horner, J.R., 1997. Nest and egg clutches of the dinosaur *Troodon formosus* and the evolution of avian reproductive traits. Nature 385, 247–250.
Varricchio, D.J., Horner, J.R., Jackson, F.D., 2002. Embryos and eggs for the Cretaceous theropod dinosaur *Troodon formosus*. Journal of Vertebrate Paleontology 22, 564–576.
Varricchio, D.J., Jackson, F.D., Jackson, R.A., Zelenitsky, D.K., 2013. Porosity and water vapor conductance of two *Troodon formosus* eggs: an assessment of incubation strategy in a maniraptoran dinosaur. Paleobiology 39, 278–296.
Varricchio, D.J., Balanoff, A.M., Norell, M.A., 2015. Reidentification of avian embryonic remains from the Cretaceous of Mongolia. PLoS One 10 (6), e0128458.
Varricchio, D.J., Kundrát, M., Hogan, J., 2018. An intermediate incubation period and primitive brooding in a theropod dinosaur. Scientific Reports 8, 12454.
Vianey-Liaud, M., Hirsch, K., Sahni, A., Sigé, B., 1997. Late Cretaceous Peruvian eggshells and their relationships with Laurasian and Eastern Gondwanian material. Geobios 30, 75–90.
Vila, B., Sellés, A.G., Beetschen, J.-C., 2017. The controversial Les Labadous eggshells: A new and peculiar dromaeosaurid (Dinosauria: Theropoda) ootype from the Upper Cretaceous of Europe. Cretaceous Research 72, 117–123.
Voris, J.T., Zelenitsky, D.K., Therrien, F., Tanaka, K., 2018. Dinosaur eggshells from the lower Maastrichtian St. Mary River Formation of southern Alberta, Canada. Canadian Journal of Earth Sciences 55, 272–282.
Wang, Q., Wang, X.-L., Zhao, Z.-K., Jiang, Y.-G., 2010. A new oogenus of Elongatoolithidae from the Upper Cretaceous Chichengshan Formation of Tiantai Basin, Zhejiang Province. Vertebrata Palasiatica 48, 111–118 (in Chinese with English summary).
Wang, S., Zhang, S., Sullivan, C., Xu, X., 2016. Elongatoolithid eggs containing oviraptorid (Theropoda, Oviraptorosauria) embryos from the Upper Cretaceous of Southern China. BMC Evolutionary Biology 16, 67.

Weishampel, D.B., Jianu, C.-M., 2011. Transylvanian Dinosaurs. Johns Hopkins University Press, Baltimore.
Weishampel, D.B., Fastovsky, D.E., Watabe, M., Varricchio, D., Jackson, F., Tsogtbaatar, K., Barsbold, R., 2008. New oviraptorid embryos from Bugin-Tsav, Nemegt Formation (Upper Cretaceous), Mongolia, with insights into their habitat and growth. Journal of Vertebrate Paleontology 28, 1110–1119.
Whitlock, J.A., D'Emic, M.D., Wilson, J.A., 2011. Cretaceous diplodocids in Asia? Re-evaluating the phylogenetic affinities of a fragmentary specimen. Palaeontology 54, 351–364.
Wiley, E.O., Lieberman, B.S., 2011. Phylogenetics: Theory and practice of phylogenetic systematics, second ed. Wiley-Blackwell, Hoboken.
Xing, L., Li, D., Harris, J.D., Bell, P.R., Azuma, Y., Fujita, M., Lee, Y.-N., Currie, P.J., 2013. A new deinonychosaurian track from the Lower Cretaceous Hekou Group, Gansu Province, China. Acta Palaeontologica Polonica 58, 723–730.
Xing, L., Lockley, M.G., Klein, H., Peng, G., Ye, Y., Jiang, S., Zhang, J., Persons IV, W.S., Xu, T., 2016. A theropod track assemblage including large deinonychosaur tracks from the Lower Cretaceous of Asia. Cretaceous Research 65, 213–222.
Xu, X., Qin, Z.-C., 2017. A new tiny dromaeosaurid dinosaur from the Lower Cretaceous Jehol Group of western Liaoning and niche differentitation among the Jehol dromaeosaurids. Vertebrata Palasiatica 55, 129–144.
Xu, X., Zhou, Z., Wang, X., 2000. The smallest known non-avian theropod dinosaur. Nature 408, 705–708.
Xu, X., Zhou, Z., Wang, X., Kuang, X., Zhang, F., Du, X., 2003. Four-winged dinosaurs from China. Nature 421, 335–340.
Xu, X., Choiniere, J.N., Pittman, M., Tan, Q., Xiao, D., Li, Z., Tan, L., Clark, J.M., Norell, M.A., Hone, D.W.E., Sullivan, C., 2010. A new dromaeosaurid (Dinosauria: Theropoda) from the Upper Cretaceous Wulansuhai Formation of Inner Mongolia, China. Zootaxa 2403, 1–9.
Xu, X., Pittman, M., Sullivan, C., Choiniere, J.N., Tan, Q.-W., Clark, J.M., Norell, M.A., Wang, S., 2015. The taxonomic status of the Late Cretaceous dromaeosaurid *Linheraptor exquisitus* and its implications for dromaeosaurid systematics. Vertebrata Palasiatica 53, 29–62.
Xu, X., Currie, P., Pittman, M., Xing, L., Meng, Q., Lü, J., Hu, D., Yu, C., 2017. Mosaic evolution in an asymmetrically feathered troodontid dinosaur with transitional features. Nature Communications 8, 14972.
Yonezawa, T., Segawa, T., Mori, H., Campos, P.F., Hongoh, Y., Endo, H., Akiyoshi, A., Kohno, N., Nishida, S., Wu, J., Jin, H., Adachi, J., Kishino, H., Kurokawa, K., Nogi, Y., Tanabe, H., Mukoyama, H., Yoshida, K., Rasoamiaramanana, A., Yamagishi, S., Hayashi, Y., Yoshida, A., Koike, H., Akishinonomiya, F., Willerslev, E., Hasegawa, M., 2017. Phylogenomics and morphology of extinct paleognaths reveal the origin and evolution of the ratites. Current Biology 27, 68–77.
Zelenitsky, D.K., 2004. Description and phylogenetic implications of extant and fossil oologic remains (Unpubl. PhD thesis). University of Calgary, p. 364.
Zelenitsky, D.K., Hills, L.V., 1996. An egg clutch of *Prismatoolithus levis* oosp.nov. from the Oldman Formation (Upper Cretaceous), Devil's Coulee, southern Alberta. Canadian Journal of Earth Sciences 33, 1127–1131.
Zelenitsky, D.K., Modesto, S.P., 2003. New information on the eggshell of ratites (Aves) and its phylogenetic implications. Canadian Journal of Zoology 81, 962–970.
Zelenitsky, D.K., Sloboda, W.J., 2005. Eggshells (Chapter 20). In: Currie, P.J., Koppelhus, E.B. (Eds.), Dinosaur Provincial Park: a spectacular ancient ecosystem revealed. Indiana University Press, Bloomington, pp. 398–404.
Zelenitsky, D.K., Therrien, F., 2008a. Unique maniraptoran egg clutch from the Upper Cretaceous Two Medicine Formation of Montana reveals theropod nesting behaviour. Palaeontology 51, 1253–1259.
Zelenitsky, D.K., Therrien, F., 2008b. Phylogenetic analysis of reproductive traits of maniraptoran theropods and its implications for egg parataxonomy. Palaeontology 51, 807–816.
Zelenitsky, D.K., Hills, L.V., Currie, P.J., 1996. Parataxonomic classification of ornithoid eggshell fragments from the Oldman Formation (Judith River Group; Upper Cretaceous), southern Alberta. Canadian Journal of Earth Sciences 33, 1655–1667.
Zelenitsky, D.K., Carpenter, K., Currie, P.J., 2000. First record of elongatoolithid theropod eggshell from North America: the Asian oogenus *Macroelongatoolithus* from the Lower Cretaceous of Utah. Journal of Vertebrate Paleontology 20, 130–138.
Zelenitsky, D.K., Therrien, F., Tanaka, K., Currie, P.J., DeBuhr, C.L., 2017a. Latest Cretaceous eggshell assemblage from the Willow Creek Formation (upper Maastrichtian – lower Paleocene) of Alberta, Canada, reveals higher dinosaur diversity than represented by skeletal remains. Canadian Journal of Earth Sciences 54, 134–140.
Zelenitsky, D.K., Therrien, F., Tanaka, K., Kobayashi, Y., DeBuhr, C.L., 2017b. Dinosaur eggshells from the Santonian Milk River Formation of Alberta, Canada. Cretaceous Research 74, 181–187.
Zhao, Z., Li, R., 1993. First record of Late Cretaceous hypsilophodontid eggs from Bayan Manduhu, Inner Mongolia. Vertebrata Palasiatica 31, 77–84 (in Chinese with English summary).
Zhao, Z., Li, Z., 1988. A new structural type of the dinosaur eggs from Anlu county, Hubei Province. Vertebrata Palasiatica 26, 107–115 (in Chinese with English summary).
Zhao, Z.-K., Mao, X.-Y., Chai, Z.-F., Yang, G.-C., Kong, P., Ebihara, M., Zhao, Z.-H., 2002. A possible causal relationship between extinction of dinosaurs and K/T iridium enrichment in the Nanxiong Basin, South China: evidence from dinosaur eggshells. Palaeogeography, Palaeoclimatology, Palaeoecology 178, 1–17.
Zhao, Z.K., Zhang, S.K., Wang, Q., Wang, X.L., 2013. Dinosaur diversity during the transition between the middle and late parts of the Late Cretaceous in eastern Shandong Province, China: Evidence from dinosaur eggshells. Chinese Science Bulletin 58, 4663–4669.
Zhou, Z., Barrett, P.M., Hilton, J., 2003. An exceptionally preserved Lower Cretaceous ecosystem. Nature 421, 807–814.

Appendices

Appendix 1

Description of characters used in the phylogenetic analysis modified from Zelenitsky (2004) and Tanaka et al. (2011).

1	Predominant ornamentation	Reticulate (0), shagreen (1), nodose (2), smooth (3), linear ridges (4).
2	Egg symmetry and shape	Spherical (0), symmetrical elongate (1), asymmetrical elongate (2).
3	Egg long axis orientation	Absent (0), subhorizontal (1), subvertical (2).
4	Clutch arrangement	Ring without central opening (0), unarranged cluster (1), ring with central opening (2), circular cluster (3).
5	Egg paring	Paired (0), unpaired (1).
6	First layer or base of shell units	Acicular (0), wedge-like (1).
7	Outer boundary of mammillary layer predominantly	Absent (0), abrupt without undulation (1), abrupt with undulation (2), gradational (3).
8	Squamatic structure of squamatic zone	Absent (0), ill-defined (1), well-defined (2).
9	External zone	Absent (0), present (1).
10	Shell units	Indiscrete (0), discrete and fan-shaped (1), discrete and columnar (2).
11	Shell units primarily	Acicular (spherulitic) (0), non-spherulitic (1).
12	Shell porosity	Porous (0), non-porous (1).
13	Pore lip around pore opening	Present (0), absent (1).
14	Pore opening in clusters	Absent (0), present (1).
15	Pore canals	Non-tubular (0), tubular (1).
16	Pore system	Irregular canals (0), multiple branching canals (1), straight with perpendicular orientation (2), straight with oblique orientation (3).

- Character 1 (predominant ornamentation): The states of *Torvosaurus* eggshell, *Reticuloolithus hirschi* and *Deinonychus* eggshell were changed into "reticulate (0)" based on original description and/or micrographs (Zelenitsky, 2004; Zelenitsky and Sloboda, 2005; Grellet-Tinner and Makovicky, 2006; Araújo et al., 2013). The state of neognaths was also modified to "smooth (3)" (Hauber, 2014).
- Character 2 (egg symmetry and shape): The state of *Torvosaurus* eggshell was changed into "?" because there is no complete egg to identify the shape (Araújo et al., 2013; Ribeiro et al., 2014). In *Prismatoolithus gebiensis*, the state was changed into "asymmetrical elongate (2)" based on the photograph (Zhao and Li, 1993). In *Triprismatoolithus stephensi*, the state was changed into "symmetrical elongate (1)" following the original description (Jackson and Varricchio, 2010). In the case of *Reticuloolithus hirschi*, this ootaxon was first coded into a matrix in Zelenitsky (2004), but the original materials of *Reticuloolithus hirschi* used in Zelenitsky (2004) and Zelenitsky and Sloboda (2005) were, in fact, mixture of *Reticuloolithus hirschi* (eggshell fragments) and *Montanoolithus strongorum* (with clutch) (Zelenitsky and Sloboda, 2005; Zelenitsky and Therrien, 2008a). Hence, clutch- and egg-shape related character (character 2–5) states of *Reticuloolithus hirschi* were changed into "?". The second character state of *Dendroolithus wangdianensis* was changed into "symmetrical elongate (1)" based on the literature (Zhao and Li, 1988).
- Character 3 (egg long axis orientation): The states of *Torvosaurus* eggshell and *Reticuloolithus hirschi* were changed into "?" because their egg shapes are unknown (see Character 2 above). The state of *Parvoolithus tortuosus* was changed into "subvertical (2)" based on Zelenitsky and Therrien (2008b).
- Character 4 (clutch arrangement): The state of *Torvosaurus* eggshell was changed into "?" because all eggs are heavily crushed so that the original arrangement of the clutch is hard to interpret (Araújo et al., 2013), and that of *Reticuloolithus hirschi* was also changed into "?" (see Character 2 above).
- Character 5 (egg pairing): The states of *Torvosaurus* eggshell and *Reticuloolithus hirschi* were changed to "?" because all eggs are crushed and/or fragmentary so that their original clutch configuration cannot be identified (Araújo et al., 2013; see Character 2 above). In *Triprismatoolithus stephensi*, the state was changed into "paired (0)" following the original description (Jackson and Varricchio, 2010).

- Character 6 (first layer or base of shell units): The states of *Torvosaurus* eggshells, oviraptorosaur eggshells, *Deinonychus* eggshells, *Reticuloolithus hirschi*, and *Arraigadoolithus patagoniensis* were changed into "acicular (0)" based on the literature (Zelenitsky and Sloboda, 2005; Grellet-Tinner and Makovicky, 2006; Zelenitsky and Therrien, 2008b; Agnolin et al., 2012; Araújo et al., 2013; Choi et al., 2019; Ribeiro et al., 2014).
- Character 7 (undulating boundary): The original matrix (Tanaka et al., 2011) was elaborated. We adopted the updated character suggested by Zelenitsky and Therrien (2008b) and changed the original character into "The outer boundary of mammillary layer predominantly", and its states as "absent (0)", "abrupt without undulation (1)", "abrupt with undulation (2)", and "gradational (3)". This new character states cover diverse boundary conditions. A similar criterion was also adopted by other researchers (e.g. the sixth character of Jin et al., 2010). The identification of character states was based on the original description and/or micrographs of each ootaxon or ooclade, as well as other data matrices (Agnolin et al., 2012; Araújo et al., 2013; Choi et al., 2019; Fernández and Salgado, 2018; Grellet-Tinner and Makovicky, 2006; Hirsch, 1994; Jackson and Varricchio, 2010; López-Martínez and Vicens, 2012; Mikhailov, 1994; Moreno-Azanza et al., 2014b; Ribeiro et al., 2014; Schweitzer et al., 2002; Skutschas et al., 2019; Tanaka et al., 2011; Varricchio and Jackson, 2004; Vila et al., 2017; Voris et al., 2018; Wang et al., 2010; Zelenitsky, 2004; Zelenitsky and Sloboda, 2005; Zelenitsky and Therrien, 2008a, b; Zhao and Li, 1993; Zhao and Li, 1988).
- Character 8 (squamatic structure of squamatic zone): The state of *Protoceratopsidovum sincerum* was changed into "absent (0)" (Mikhailov, 1994, 2014; Moreno-Azanza et al., 2014a).
- Character 9 (external zone): The states of *Troodon* eggshells and *Prismatoolithus levis* were changed into "present (1)" (Choi et al., 2019; Funston and Currie, 2018; Jackson et al., 2010; Skutschas et al., 2019; Varricchio and Jackson, 2004; Zelenitsky and Therrien, 2008b). In addition, that of *Gobioolithus minor* was changed into "absent (0)" based on the literature (Choi et al., 2019; Mikhailov, 2014).
- Character 10 (shell units): The state of *Torvosaurus* eggshell was changed into "discrete and fan-shaped (1)" based on the literature (Araújo et al., 2013; Ribeiro et al., 2014). In addition, the states of *Lourinhanosaurus* eggshell and *Preprismatoolithus coloradensis* were also changed into "discrete and columnar (2)" (Hirsch, 1994; Ribeiro et al., 2014). In *Gobioolithus minor*, the state was changed into "discrete and columnar (2)" based on the literature (Choi et al., 2019). In *Tantumoolithus lenis*, it was modified into "indiscrete (0)" because the original description regarded this ootaxon as 'ratite morphotype' (Fernández and Salgado, 2018), which is characterized by indiscrete shell units (Mikhailov et al., 1996; Mikhailov, 1997a) and no columnar shell unit boundaries were seen in the original figures.
- Character 11 (shell units primarily): The state of *Torvosaurus* eggshell was modified to "acicular (spherulitic) (0)" based on the literature (Araújo et al., 2013; Ribeiro et al., 2014).
- Character 12 (shell porosity): The state of *Torvosaurus* eggshell was modified to "porous (0)" following the original literature (Araújo et al., 2013) and so did *Dendroolithus wangdianensis* (Zhao and Li, 1988).
- Character 13 (pore lip): The states were all reversed ("0" → "1" and "1" → "0") because only *Preprismatoolithus coloradensis* and *Lourinhanosaurus* eggshell have pore lips around their pore openings in the original matrix of Zelenitsky (2004). However, *Arragadoolithus patagoniensis* has a pore lip around the pore openings (Agnolin et al., 2012, fig. 10C) so that its character state was changed into "present (0)".
- Character 14 (pore opening in clusters): The state of *Torvosaurus* eggshell was modified into "absent (0)" following the original micrograph (Araújo et al., 2013).
- Character 15 (pore canals): The states of *Montanoolithus strongorum* and *Triprismatoolithus stephensi* were modified into "?" because it was not presented in the original description (Zelenitsky and Therrien, 2008a; Jackson and Varricchio, 2010) but was coded in Vila et al. (2017) without proper explanation.
- Character 16 (pore system): The states of *Montanoolithus strongorum* and *Triprismatoolithus stephensi* were modified to "?" because they were not presented in the original descriptions (Zelenitsky and Therrien, 2008a; Jackson and Varricchio, 2010) but was coded in Vila et al. (2017) without proper explanation.

A coding for *Prismatoolithus ilekensis* was supplemented from Skutschas et al. (2019). A coding for *Paraelongatoolithus reticulatus* was made from the original description of Wang et al. (2010). *Sankofa pyrenaica* was coded into the matrix in order to encompass diverse oogenera of the Prismatoolithidae. Our new coding was based on the original description of López-Martínez and Vicens (2012), except for characters 9 and 10. Although they described the shell unit of *Sankofa pyrenaica* as 'prismatic', the thin section images clearly show that the rugged grain boundaries in the continuous layer are very similar to those of rhea (paleognath) eggshells (Choi et al., 2019), which is coded as "indiscrete (0)". We think that the 'prismatic' layer at the inner part of the *Sankofa pyrenaica* described in López-Martínez and Vicens (2012) is, in fact, the extended outer region of the mammillary layer. In addition, they contended that the external zone does not exist. However, Choi et al. (2019) proposed that the linear grain boundaries at the external end of the eggshell can be used to diagnose the existence of the external zone. It is clear that the outer end of the *Sankofa pyrenaica* is characterized by the linear grain boundaries unlike rugged grain boundaries of squamatic ultrastructure lying below. Therefore, it is highly probable that *Sankofa pyrenaica* has an external zone so that the ninth character (external zone) was coded as "present (1)".

Maiasaura eggshell was used as an outgroup in the phylogenetic analysis (e.g. Zelenitsky, 2004; Tanaka et al., 2011). However, we propose that the egg of *Torvosaurus* would be a more appropriate outgroup. According to literature, "A character assigned to the outgroup node would be the character hypothesized to be present in the ancestor of the ingroup and its sister group." (Wiley and Lieberman, 2011, p. 159). Because all ootaxa included in the phylogenetic analysis are dinosaur eggshells (both saurischian and ornithischian), in a strict sense, an ideal outgroup should be assigned to the egg fossil laid by non-dinosaurian Dinosauromorpha or its closely related taxon. However, no dinosauromorph egg fossil was reported so that it would be realistic to find a candidate of outgroup among the most primitive and oldest dinosaur egg fossil known assuming that it still preserved ancestral characters. This inductive reasoning could be justified by the fact that eggshell microstructure is rather conservative and evolves slowly (Mikhailov, 1997b; Moreno-Azanza et al., 2017; Athanasiadou et al., 2018). Recently, Stein et al. (2019) reported the oldest (Early Jurassic) dinosaur eggshells from Africa, Asia, and South America. Although these sauropodomorph eggshells provide meaningful primitive state of amniotic eggs, we could not put their characters into the matrix due to lack of concomitant information of them. Hence, we believe that a well-preserved ootaxon from the Late Jurassic deposit can be a better outgroup rather than Early Jurassic eggs and frequently used Late Cretaceous ootaxon (i.e. egg of *Maiasaura*) because there is approximately 80 Myr time gap between the eggs of *Maiasaura* and *Torvosaurus*. Between the two Late Jurassic ootaxa (egg of *Torvosaurus* and *Preprismatoolithus*), the former would be a better outgroup because the microstructures of *Preprismatoolithus* are more similar to those of maniraptoran eggshells compared to other dinosaur eggshells. The similarity may be homologic or homoplastic to derived maniraptoran eggshells (see above). Hence, we selected the egg of *Torvosaurus* as an outgroup.

Appendix 2

Data matrix used in this study modified from Tanaka et al. (2011), Vila et al. (2017), Skutschas et al. (2019), and Fernández and Salgado (2018).

	1	2	3	4	5	6	7	8	9	10	11	12	13	14	15	16
Egg of *Maiasaura*	0	0	0	?	?	0	0	0	0	0	0	0	1	0	0	0
Paraspheroolithus irenensis	0	0	0	0	?	0	0	0	0	0	0	0	1	0	0	0
Spheroolithus spheroids	0	0	0	0	?	0	0	0	0	0	0	0	1	0	0	0
Faveoloolithus ningxianensis	1	0	0	1	?	0	0	0	0	0	0	0	1	0	0	1
Egg of titanosaurs	2	0	0	1	?	0	0	0	0	1	0	0	1	0	1	2
Megaloolithus mammilare	2	0	0	1	?	0	0	0	0	1	0	0	1	0	1	2
Megaloolithus rahioliensis	2	0	0	1	?	0	0	0	0	1	0	0	1	0	1	2
Egg of *Torvosaurus*	0	?	?	?	?	0	0	0	0	1	0	0	?	0	0	1
Egg of *Lourinhanosaurus*	3	1	1	?	1	0	3	1	0	2	1	0	0	0	1	3
Preprismatoolithus coloradensis	3	1	1	2	0	0	3	1	0	2	1	0	0	0	1	3
Macroolithus rugustus	4	1	1	2	0	0	2	1	0	0	1	1	1	0	1	2
Elongatoolithus elogatus	4	1	1	2	0	0	2	1	0	0	1	1	1	0	1	2
Eggs of sm. oviraptorids	4	1	1	2	0	0	2	1	0	0	1	1	1	0	1	2
Eggs of lg. oviraptorids	4	1	1	?	?	0	2	1	0	0	1	1	1	0	1	2
Macroelongatoolithus xixiaensis	4	1	1	2	0	0	2	1	0	0	1	1	1	0	1	2
Macroelongatoolithus carlylei	4	?	?	?	?	0	2	1	0	0	1	1	1	0	1	2
Luanchuan eggshells	4	?	?	?	?	0	2	1	0	0	1	1	1	0	1	2
Eggs of *Deinonychus*	0	?	?	?	?	0	1	1	0	0	1	1	1	0	1	2
Reticuloolithus hirschi	0	?	?	?	?	0	1	1	0	0	1	1	1	0	1	2

Appendix 2 (*continued*)

	1	2	3	4	5	6	7	8	9	10	11	12	13	14	15	16
Reticuloolithus acicularis	0	?	?	?	?	0	1	1	0	0	1	1	1	0	1	2
Paraelongatoolithus reticulatus	0	1	?	?	?	0	1	1	0	0	1	1	1	1	1	2
Prismatoolithus levis	3	2	2	3	0	1	3	1	1	2	1	1	1	1	1	2
Eggs of *Troodon*	3	2	2	3	0	1	3	1	1	2	1	1	1	1	1	2
Prismatoolithus gebiensis	3	2	2	3	0	1	3	1	0	2	1	1	1	0	1	2
Prismatoolithus ilekensis	3	2	?	?	?	1	3	1	1	2	1	1	1	?	1	2
Protoceratopsidovum sincerum	3	2	2	3	0	1	3	0	0	2	1	1	1	0	1	2
Trigonoolithus amoae	2	?	?	?	?	1	3	1	1	2	1	1	1	0	1	2
Montanoolithus strongorum	0	2	1	2	0	1	3	1	0	2	1	1	1	0	?	?
Montanoolithus labadousensis	0	?	?	?	?	1	3	1	0	2	1	1	1	0	1	2
Triprismatoolithus stephensi	1	1	?	?	0	1	3	1	1	2	1	1	1	0	?	?
Arraigadoolithus patagoniensis	1	?	?	?	?	0	3	1	1	2	1	1	0	0	0	3
Sankofa pyrenaica	3	2	2	?	?	1	3	1	1	0	1	?	1	0	1	?
Parvoolithus tortuosus	3	2	2	?	1	1	1	2	1	2	1	1	1	0	1	2
Gobioolithus minor	3	2	2	?	1	1	3	2	0	2	1	1	1	0	1	2
Tantumoolithus lenis	3	2	?	?	?	1	1	2	0	0	1	1	1	0	1	2
MUCPv-350 Neuquen	3	2	2	1	1	1	3	2	1	2	1	1	1	0	1	?
Eggs of paleognaths	3	1	1	3	1	1	1	2	1	0	1	1	1	0	1	2
Eggs of neognaths	3	2	1	3	1	1	3	2	1	2	1	1	1	0	1	2
Dendroolithus wangdianensis	1	1	0	3	1	1	3	?	0	2	1	0	1	0	0	1
Egg of therizinosaurs	1	0	0	3	1	1	0	?	0	2	1	1	1	0	0	1